TriDurLE

National Center for Transportation Infrastructure Durability & Life-Extension

Project ID: 2022-WSU-03

Life-Cycle Fire Performance Assessment and Enhancement of Reinforced Concrete Bridges in Chloride-laden Environments

Final Report

by

Ji Yun Lee, Associate Professor, Washington State University
Xianming Shi, Professor, University of Miami
Jialuo He, Research Assistant Professor, Washington State University
Sailong Hou, Postdoctoral Research Associate, Washington State University
Vishnupriya Jonnalagadda, Postdoctoral Researcher, Florida State University

for

National University Transportation Center TriDurLE
Department of Civil & Environmental Engineering
405 Spokane Street PO Box 642910
Washington State University Pullman, WA 99164-2910

Date
January 23, 2026

Acknowledgements

The work presented in this report was sponsored by the National Center for Transportation Infrastructure Durability & Life Extension (TriDurLE). This support is gratefully acknowledged.

Disclaimer

Table of Contents

Contents

List of Figures

List of Tables

Executive Summary

The goal of this project is to assess and enhance the life-cycle fire performance of reinforced concrete (RC) bridges in chloride-laden environments. The project consists of two phases: (a) experiments that aim to assess the degradation of steel–concrete bond performance in RC systems subjected to combined corrosion and thermal exposure; and (b) a methodological framework that assesses and enhances the long-term fire performance of RC bridges in chloride-laden environments under deep uncertainty.

The first phase focuses on a comparative evaluation of Portland limestone cement concrete (PLC) and geopolymer concrete (GPC), with emphasis on their bond behavior with reinforcing steel under multi-hazard conditions representative of long-term service environments for transportation infrastructure. Pull-out tests were conducted on RC specimens incorporating deformed steel bars and subjected to four corrosion states (no corrosion, mild corrosion, medium corrosion, and severe corrosion) in combination with three thermal exposure conditions (room temperature, 300 °C, and 800 °C). Corrosion states were established and verified through electrochemical measurements, including open circuit potential (OCP) and corrosion current density (CCD), ensuring consistent classification of corrosion severity. Thermal exposure was applied using a controlled high-temperature heating system designed to simulate fire-related temperature histories relevant to bridge infrastructure. Full load–slip responses were obtained under displacement-controlled pull-out testing. A systematic data screening procedure was implemented to exclude non-physical responses and retain meaningful bond behavior. The peak pull-out load was adopted as the primary quantitative indicator of steel–concrete bond performance, as it represents the maximum mobilized interfacial resistance regardless of post-peak response characteristics.

The experimental results demonstrate that steel–concrete bond degradation is governed by a strong interaction between corrosion severity and exposure temperature. For both PLC and GPC specimens, exposure to 800 °C results in substantial reductions in peak pull-out load across all corrosion levels, indicating severe impairment of bond capacity under extreme thermal conditions. However, the degradation pathways differ between the two materials. PLC exhibits pronounced interaction effects, including non-monotonic interaction effects at lower temperatures and abrupt bond degradation at high temperatures, particularly under medium and severe corrosion. In contrast, GPC shows a more monotonic on average reduction in bond capacity across the corrosion–temperature domain, with reduced scatter in test results. These findings confirm that pre-existing corrosion significantly amplifies temperature-induced bond degradation, and that approaches considering temperature effects alone may underestimate bond loss in aging reinforced concrete structures. The experimental database developed in this study

provides a robust foundation for subsequent probabilistic modeling and reliability-based assessment of bond performance under TriDurLE Objective 2, supporting life-cycle fire performance evaluation of reinforced concrete bridges in chloride-laden environments.

The second phase introduces a comprehensive methodological framework to evaluate and enhance the long-term fire performance of RC bridges exposed to chloride-laden environments under deep uncertainty. Recognizing the limitations of conventional deterministic and probabilistic models in addressing long-range, complex uncertainties, the proposed framework integrates Information Gap Decision Theory (IGDT) with Dynamic Adaptive Policy Pathways (DAPP) to support both robust and adaptive decision-making. The IGDT component enables a structured exploration of material robustness by accounting for uncertainty envelopes around key parameters such as material degradation and environmental exposure. The envelope-bound IG model offers a flexible representation of parameter uncertainty and interdependence, making it well-suited for infrastructure applications with limited or imprecise data. The robustness metric derived through IGDT supports preliminary material screening based on performance under worst-case conditions. To complement this, the DAPP framework is adapted to incorporate robustness considerations into the selection of forecast and decision horizons. The approach accounts for evolving system needs by identifying tipping points related to fire performance degradation, policy shifts, cost constraints, and technological change. An optimization model is introduced to guide cost-effective timing of interventions while ensuring that structural and fire performance thresholds are met throughout the lifecycle. This integrated IGDT-DAPP framework offers a proactive and flexible decision-support approach, in contrast to static or pre-defined maintenance planning strategies. Finally, a simplified conceptual example demonstrates the application of the methodology, illustrating how robustness varies across uncertainty levels and informing the selection of maintenance actions and adaptation points.

Chapter 1. Introduction

1.1 Problem Statement

Reinforced concrete (RC) bridges constitute a critical component of transportation infrastructure in chloride-laden environments, where long-term exposure to deicing salts and marine aerosols promotes corrosion of reinforcing steel. Concurrently, bridges are increasingly required to maintain structural integrity under extreme thermal events, such as vehicle fires, wildfires, and post-earthquake fires. These combined environmental stressors pose significant challenges to the durability and safety of RC bridge systems and highlight the need for performance-based evaluation of material degradation mechanisms under multi-hazard conditions. Steel corrosion has been widely recognized as a dominant factor governing the long-term deterioration of RC structures, leading to cracking, loss of cross-sectional area, and degradation of steel–concrete bond. Separately, elevated temperatures are known to impair concrete microstructure, reduce mechanical strength, and weaken interfacial properties between steel and concrete. However, in real service conditions, corrosion and thermal exposure rarely occur in isolation. Corrosion-induced damage accumulated during long-term service may substantially alter the response of RC systems to subsequent fire exposure, particularly with respect to steel–concrete bond performance, which plays a critical role in force transfer, load redistribution, and overall structural resilience. Despite extensive research on corrosion-induced degradation and fire-induced damage individually, the coupled effects of corrosion severity and elevated temperature on steel–concrete bond behavior remain insufficiently quantified, especially for alternative cementitious systems. Existing design approaches and post-fire assessment methods often consider temperature effects without explicitly accounting for pre-existing corrosion, which may result in unconservative estimates of residual bond capacity and structural performance. In parallel, the growing interest in geopolymer concrete (GPC) as a low-carbon alternative to Portland cement–based materials has raised important questions regarding its long-term durability and performance under combined environmental hazards. While GPC has demonstrated promising resistance to high temperatures and aggressive chemical environments, its steel–concrete bond behavior under coupled corrosion and thermal exposure has not been systematically evaluated or benchmarked against conventional Portland limestone cement concrete (PLC).

To predict the long-term behavior of concrete, deterministic models [1,2] have been widely used to predict single-point performance indicators by integrating physics-based deterioration functions with empirical data. However, results from such models are typically derived under best-estimate assumptions, which may deviate significantly from real-world behavior due to inherent aleatory and epistemic

uncertainties. To address the issues with the deterministic approach, a limited number of studies have proposed probabilistic performance models that consider the combined influence of corrosion and fire. Nevertheless, these approaches still fall short of fully capturing deep uncertainties—which stem from long-term material behavior, future climate conditions, and the performance of emerging materials. Deep uncertainty refers to conditions where probability distributions, system behavior, or future scenarios are not well known or even knowable. When considering infrastructure systems with service lives spanning several decades, the inability to account for deep uncertainty limits the reliability of traditional performance predictions. Addressing these challenges requires a dynamic and adaptive planning approach that moves beyond fixed maintenance schedules. The literature highlights the significance of forecast and decision horizons in adaptive infrastructure management, underscoring the need for flexible and responsive strategies that can evolve with emerging conditions [3,4]. Adaptive planning is therefore indispensable, offering a mechanism to integrate new information and adjust decisions over time, while explicitly addressing deep uncertainties [5-9].

Within this context, there is a clear need for (a) controlled experimental data that quantitatively characterize steel–concrete bond degradation across multiple corrosion states and thermal exposure levels, and that enable direct comparison between conventional and alternative concrete systems and (b) the development of a robust, dynamic, adaptive decision framework that assesses and enhances the long-term fire performance of RC bridges in chloride-laden environments under deep uncertainty. Addressing this gap is essential for advancing performance-based assessment frameworks and for supporting the life-cycle evaluation of RC bridge infrastructure under the objectives of the TriDurLE program.

1.2 Objectives

The overarching goal of this proposed project is to quantify and enhance the life-cycle fire performance of RC bridges in chloride-laden environments. This goal is well aligned with the TriDurLE mission in “improving the durability and extending the life of transportation infrastructure”. The project has the potential to integrate the five interrelated thrust areas of TriDurLE into the proposed life-cycle fire performance assessment and enhancement framework. To achieve this goal, the following objectives were met.

- Establish reproducible corrosion states for reinforcing steel representative of different stages of long-term deterioration, ranging from no corrosion (or corrosion initiation) to severe corrosion, using electrochemical characterization methods including open circuit potential

(OCP) and corrosion current density (CCD).

- Quantify the steel–concrete bond behavior of reinforced specimens subjected to multiple corrosion states in combination with controlled thermal exposure conditions, including ambient temperature, moderate elevated temperature (300 °C), and severe high-temperature exposure (800 °C).
- Characterize and compare the bond degradation mechanisms of Portland limestone cement concrete (PLC) and geopolymer concrete (GPC) under coupled corrosion–temperature conditions, with particular emphasis on differences in degradation trends, sensitivity to corrosion severity, and temperature-induced interaction effects.
- Identify a robust bond performance indicator suitable for multi-hazard assessment by analyzing full load–slip responses from pull-out tests and adopting peak pull-out load as a consistent and physically meaningful metric for comparing corrosion and temperature effects.
- Develop a comprehensive experimental database that captures the coupled influence of corrosion severity and thermal exposure on bond performance, providing a quantitative basis for reliability-based modeling and life-cycle fire performance evaluation under TriDurLE Objective 2.
- Implement info-gap decision theory (IGDT) to address deep uncertainty by providing a robustness-centered approach to decision-making.
- Develop a dynamic adaptive decision planning model to increase a temporal dimension to the decision-making process and combine it with IGDT.
- Demonstrate the proposed methodological framework with a simple conceptual example.

1.3 Expected Contributions

This study is expected to contribute to the TriDurLE program by providing a systematic and quantitative understanding of steel–concrete bond degradation under coupled corrosion and thermal exposure, addressing a critical knowledge gap in multi-hazard performance assessment of reinforced concrete bridge infrastructure.

The primary expected contributions of this work include:

- A quantitative corrosion-state framework for bond assessment, in which corrosion severity is defined and verified using electrochemical indicators (OCP and CCD) rather than exposure time alone. This framework enables consistent classification of corrosion damage and improves the reliability of multi-

hazard performance evaluation.

- An experimental database capturing coupled corrosion–temperature effects on bond performance, covering multiple corrosion states and thermal exposure levels for both PLC and GPC systems. The database provides high-resolution insight into how corrosion severity modifies temperature-induced bond degradation.
- A direct comparison between conventional and alternative cementitious systems, elucidating differences in bond degradation pathways between Portland limestone cement concrete and geopolymer concrete under combined environmental stressors. These comparisons support informed material selection and performance-based design considerations for future bridge infrastructure.
- Identification of peak pull-out load as a robust bond performance indicator for multi-hazard conditions, supported by full load–slip characterization and systematic data screening. This contribution facilitates consistent interpretation of experimental results and supports subsequent modeling efforts.
- A foundational dataset for probabilistic and life-cycle modeling, enabling the integration of corrosion and fire effects into reliability-based assessment frameworks under TriDurLE Objective 2.
- A methodological framework that assesses and enhances the long-term fire performance of RC bridges in chloride-laden environments under deep uncertainty.

1.4 Report Overview

This report is organized into five chapters. Chapter 1 (a) introduces the background and motivation of the study, (b) defines the problems associated with steel–concrete bond degradation under coupled corrosion and thermal exposure as well as the assessment of long-term performance of PLC and GPC, and (c) outlines the objectives and expected contributions of the work within the TriDurLE framework.

Chapter 2 provides a focused review of relevant literature on corrosion-induced bond degradation, temperature effects on reinforced concrete, and prior studies addressing multi-hazard interactions affecting steel–concrete bond behavior.

Chapter 3 consists of two sections: (a) the experimental program and methodology, including specimen design, corrosion conditioning and electrochemical characterization, thermal exposure protocols, pull-out testing procedures, and data processing methods used to quantify bond performance; and (b) a robust, dynamic, adaptive decision framework that assesses and enhances the long-term fire performance of RC bridges in chloride-laden environments under deep uncertainty.

Chapter 4 presents and discusses the experimental results, with emphasis on the coupled effects of

corrosion severity and temperature on steel–concrete bond behavior. Comparative performance of PLC and GPC is examined, and key interaction effects are identified. Moreover, a simple illustrative example of the proposed decision framework is introduced.

Chapter 5 summarizes the main findings of the study, highlights their implications for multi-hazard performance assessment of reinforced concrete bridge infrastructure, and outlines how the project results support subsequent modeling and reliability-based evaluation under TriDurLE Objective 2.

Chapter 2. Literature Review

Steel–concrete bond is a governing mechanism for force transfer and composite action in reinforced concrete (RC) systems and has been widely recognized as a critical factor influencing durability, load redistribution, and post-event structural performance. Within the TriDurLE framework, deterioration of bond performance is of particular concern for bridge infrastructure exposed to chloride-induced corrosion during long-term service and extreme thermal events such as vehicle or post-earthquake fires [3,10,11]. Chloride-induced corrosion of reinforcing steel is a primary deterioration mechanism in RC bridges exposed to deicing salts and marine environments. Once the chloride concentration at the steel surface exceeds a critical threshold, depassivation occurs and corrosion products accumulate at the steel–concrete interface, inducing tensile stresses in the surrounding concrete cover [12,13]. Numerous experimental studies[8,14,15] have shown that corrosion affects steel–concrete bond through competing mechanisms. At low corrosion levels, limited accumulation of corrosion products may increase interfacial friction and confinement, resulting in marginal increases or stabilization of bond resistance. As corrosion progresses, however, cracking of the concrete cover, degradation of rib geometry, and loss of confinement dominate, leading to substantial reductions in bond capacity and increased scatter in bond response [16-18]. These trends have been consistently reported for deformed reinforcing bars embedded in conventional Portland cement–based concretes.

Characterization of corrosion severity has traditionally relied on exposure duration or mass loss measurements. However, as emphasized in the TriDurLE proposal, such indicators do not necessarily reflect corrosion activity or damage state. Electrochemical techniques, including open circuit potential (OCP) and corrosion current density measurements obtained from linear polarization resistance (LPR), have therefore been increasingly adopted to quantify corrosion state in a mechanistically meaningful and reproducible manner [19-21]. These approaches enable consistent comparison of corrosion severity across specimens and studies. Exposure to elevated temperatures during fire events has been shown to significantly degrade steel–concrete bond performance. Thermal damage arises from deterioration of concrete microstructure, loss of mechanical interlock and chemical adhesion at the steel–concrete interface, and thermally induced cracking caused by differential thermal expansion between steel and concrete[22,23]. Experimental investigations [24-26] have demonstrated that bond degradation accelerates with increasing temperature, with moderate temperature exposure causing gradual reduction in bond strength and severe exposure leading to abrupt bond loss and changes in failure mode. Most existing studies, however, have focused on uncorroded specimens, implicitly assuming intact interfacial

conditions prior to fire exposure. As highlighted in the TriDurLE proposal, post-fire assessment methods commonly adopt temperature-only reduction factors derived from such tests, which may not adequately represent the residual bond capacity of structures that have experienced long-term corrosion prior to fire events [26-28].

In real service environments, corrosion and thermal exposure act sequentially or concurrently rather than independently. Corrosion-induced cracking and interfacial degradation accumulated during long-term service can significantly modify the response of RC systems to subsequent fire exposure. Recent studies [29,30] have begun to recognize that pre-existing corrosion may amplify temperature-induced bond degradation and increase uncertainty in residual bond performance. Despite this recognition, available experimental data addressing coupled corrosion–temperature effects remain limited. Existing studies are often restricted to a single corrosion level or a narrow temperature range, and systematic frameworks linking corrosion state, thermal exposure, and bond degradation are largely absent. This limitation has been explicitly identified in the TriDurLE proposal as a critical barrier to performance-based, multi-hazard assessment of RC bridge infrastructure. In response to sustainability and decarbonization objectives, geopolymer concrete (GPC) has emerged as a promising alternative to conventional Portland cement–based materials. Previous studies [31-33] have reported favorable high-temperature resistance, reduced spalling potential, and improved chemical durability of geopolymer systems compared with ordinary Portland cement concretes. However, as noted in the TriDurLE proposal, the steel–concrete bond behavior of GPC under combined corrosion and thermal exposure has not been systematically investigated. Existing studies[21,34] on geopolymer materials have primarily focused on mechanical properties or thermal resistance, with limited attention to interfacial behavior and bond degradation mechanisms under multi-hazard conditions. Direct experimental comparison between GPC and Portland limestone cement concrete (PLC) in the context of coupled corrosion–temperature effects remains scarce.

Based on the literature reviewed above and the gaps identified in the TriDurLE proposal, the following needs are evident:

- Quantitative experimental data on steel–concrete bond degradation under combined corrosion and elevated temperature.
- Consistent, electrochemically based characterization of corrosion severity.
- Direct comparison of conventional and alternative cementitious systems under multi-hazard conditions.

- Experimental foundations suitable for reliability-based and life-cycle performance modeling of RC bridges.

The present study directly addresses these gaps by integrating electrochemically defined corrosion states, controlled thermal exposure, and standardized pull-out testing within the TriDurLE Objective 1 framework.

Chapter 3. Methodology

3.1 Experiment

The experimental program was designed to systematically quantify steel–concrete bond degradation under coupled corrosion and thermal exposure, in alignment with TriDurLE Objective 1. A factorial framework was adopted in which reinforced concrete specimens were subjected to multiple corrosion states and exposure temperatures. Two concrete systems—PLC and GPC—were investigated to enable direct comparison between conventional and alternative cementitious materials.

The experimental workflow consisted of specimen fabrication, corrosion conditioning and electrochemical characterization, controlled thermal exposure, displacement-controlled pull-out testing, and post-processing of load–slip data to quantify bond performance.

3.1.1 Materials and Specimen Design

Two concrete systems were investigated in this study: PLC and GPC. The PLC mixture was designed using a conventional Portland limestone cement binder, while the GPC mixture employed a fly ash–based binder activated by alkaline and sulfate components. The mixture proportions for both systems are summarized in Table 1, where all materials are reported in kg/m^3 to facilitate direct comparison. To ensure comparability between the two concrete systems, the binder content and aggregate-to-binder ratio were kept identical for PLC and GPC. Specifically, both mixtures employed a binder content of 536 kg/m^3 and a sand-to-binder ratio of 3.0. Differences between the two systems were limited to the type of binder and the presence of activators and admixtures required for geopolymerization in the GPC mixture.

Table. 1 Mixture proportions of PLC and GPC (kg/m^3)

Category	Material	PLC (kg/m^3)	GPC (kg/m^3)
Binder	Cement / Fly ash	536	536
Aggregate	Sand	1607.9	1607.9
Mixing water	Free water	214.3	102.7
	SSD water	20.3	20.3
Activator / additives	Water glass	–	32.1
	Quick lime	–	19.3
	Na_2SO_4	–	5.4
	HRWRA	–	26.8
	Triisopropanolamine (TIPA)	–	6.4
	GO	–	5.4
Total		2378.8	2361

The PLC mixture consisted of cement, sand, and mixing water, with additional water corresponding

to the saturated surface-dry (SSD) condition of the sand. The GPC mixture utilized fly ash as the primary binder, in combination with water glass, quick lime, sodium sulfate, and chemical admixtures, including a high-range water-reducing admixture (HRWRA), triisopropanolamine (TIPA), and graphene oxide (GO). For the GPC mixture, all activators and admixtures were introduced based on as-batched mass, consistent with the project proposal.

Reinforced concrete specimens were designed for pull-out testing to evaluate steel–concrete bond behavior. Deformed steel reinforcing bars were centrally embedded in prismatic concrete specimens, as illustrated in Fig. 1, with embedment length (70mm) selected to promote bond-controlled behavior while minimizing global splitting failure. The specimen geometry and embedment configuration were maintained consistently across all test groups to isolate the effects of corrosion severity and thermal exposure.

All specimens were cast and cured under identical conditions prior to corrosion conditioning. This approach minimized variability associated with early-age material differences and ensured that observed differences in bond performance could be attributed primarily to corrosion state, thermal exposure, and concrete system type.

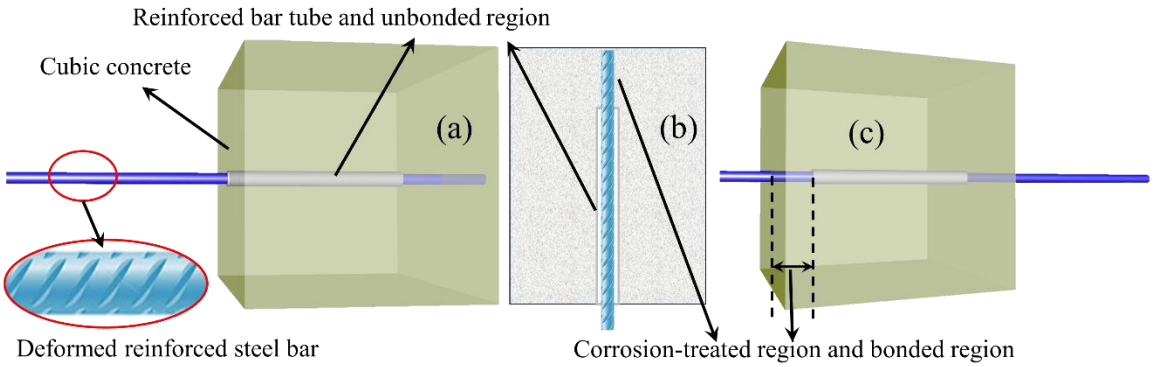

Fig. 1 Schematic illustration of the sample preparation

3.1.2 Corrosion Conditioning and Definition of Corrosion States

Corrosion conditioning was applied to generate four discrete corrosion states representative of progressive deterioration of reinforcing steel during long-term service: no corrosion, mild corrosion, medium corrosion, and severe corrosion. These corrosion states were defined to capture increasing levels of corrosion activity and steel–concrete interfacial degradation relevant to chloride-exposed reinforced concrete infrastructure. Accelerated corrosion was induced using a sodium chloride–based conditioning protocol in a salt spray chamber, as shown in Fig. 2a, to promote controlled corrosion development at the

steel–concrete interface. Conditioning duration was varied nominally (0, 3, 6, and 9 days) to facilitate progressive corrosion development, as illustrated in Fig. 2b. However, corrosion severity was not defined solely based on exposure duration. Instead, corrosion states were quantitatively characterized using electrochemical response parameters, consistent with the methodology outlined in the TriDurLE proposal.

Electrochemical measurements, including open circuit potential (OCP) and corrosion current density (CCD marked as i_{corr} calculated by Eq. 2), were employed to monitor corrosion activity and to inform the classification of corrosion severity. Measurements were conducted using a standard three-electrode electrochemical setup (Fig. 2c), with the reinforcing steel acting as the working electrode. OCP provides an indicator of the thermodynamic tendency for corrosion initiation, while the corrosion current density reflects the rate of active corrosion. The combined interpretation of these parameters enables a mechanistically meaningful assessment of corrosion state that is independent of conditioning duration alone. Corrosion current density was estimated from linear polarization resistance (LPR) measurements. During LPR testing, the reinforcing steel was polarized within ±15 mV of its open circuit potential at a scan rate of 0.1667 mV/s, ensuring that measurements remained within the linear polarization region. The polarization resistance, R_p, was determined as the slope of the polarization curve according to:

$$R_P = \frac{\Delta V}{\Delta i} \qquad \text{Eq. (1)}$$

where ΔV and Δi represent the applied potential perturbation at the working electrode and the corresponding change in current density, respectively. The corrosion current density, i_{corr}, was subsequently estimated using the Stern–Geary relationship:

$$i_{corr} = \frac{B}{R_P} \qquad \text{Eq. (2)}$$

where B is the Stern–Geary constant, assumed to be 26 mV for reinforcing steel in concrete [35].

Based on the measured electrochemical response, specimens conditioned for nominal durations of 0, 3, 6, and 9 days were mapped to the four corrosion states defined above in Fig. 2(b). As summarized in Table 2, specimens classified as no corrosion exhibited relatively noble OCP values and very low corrosion current density, indicative of passive steel conditions. Mild corrosion corresponded to moderately negative OCP values and low i_{corr}, reflecting early-stage corrosion initiation. Medium corrosion was associated with more negative OCP values and moderate corrosion current density, indicating sustained active corrosion. Severe corrosion exhibited highly negative OCP values and high corrosion current density, corresponding to advanced active corrosion with pronounced steel–concrete interfacial degradation. This electrochemically informed classification, established under a chloride-based

conditioning environment, ensured consistency between measured corrosion activity and the corrosion severity categories used in subsequent analysis, while avoiding reliance on fixed threshold values or conditioning duration alone. Specimens conditioned for nominal durations of 0, 3, 6, and 9 days were initially assigned to four corrosion-state categories and subsequently verified and characterized using OCP and LPR-derived i_{corr}. Exposure duration was used as a conditioning control parameter, while corrosion state classification was finalized based on electrochemical response.

(a) Salt spray chamber

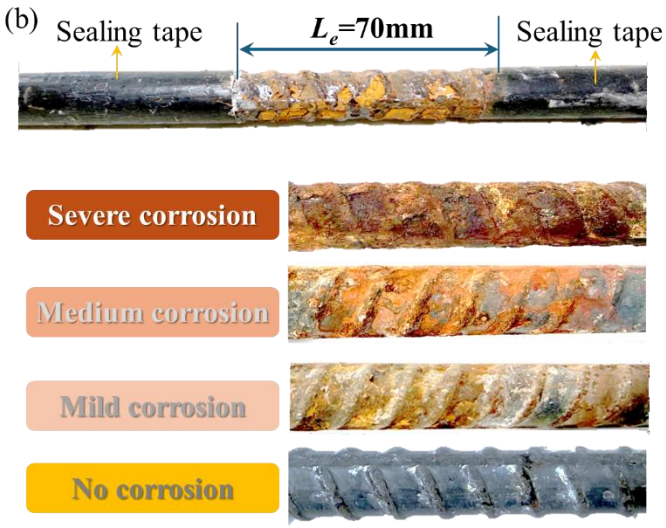

(b) Corrosion conditions of steel fibers

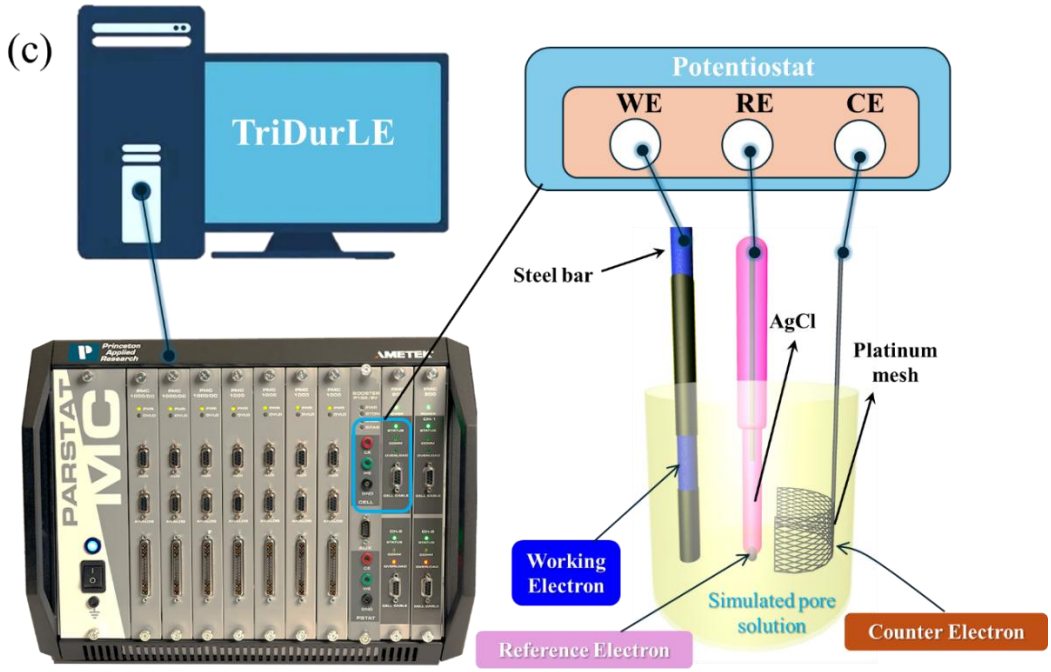

(c) Three-electrode Setup for OCP and corrosion current density measurements.

Fig. 2 Experimental setup and corrosion characterization

Table. 2 Definition of corrosion states for reinforcing steel

Corrosion state	Conditioning duration (days)	OCP (V vs. reference)	CCD (μA/cm²)	Reinforcement condition	Description
No corrosion	0	Relatively noble	Very low	Passive steel surface	Steel remains in passive condition with no measurable corrosion activity; no visible corrosion products or interfacial damage
Mild corrosion	3	Typically more negative than baseline	Low	Early-stage corrosion initiation	Onset of depassivation with limited corrosion activity; minimal accumulation of corrosion products and negligible cracking
Medium corrosion	6	Generally negative	Moderate	Active corrosion	Sustained corrosion activity with noticeable corrosion products at the steel–concrete interface; microcracking may develop
Severe corrosion	9	Often negative with higher variability	High	Advanced active corrosion	Intense corrosion activity with significant accumulation of corrosion products and pronounced interfacial degradation

3.1.3 Thermal Exposure Protocol

Specimens were subjected to one of three thermal exposure conditions: room temperature (22 °C, no heating), 300 °C, and 800 °C. These temperature levels were selected to represent no-fire conditions, moderate thermal damage, and severe thermal damage scenarios relevant to fire exposure in reinforced concrete infrastructure. High-temperature exposure was conducted using a liquid natural gas–fueled heating system, as schematically illustrated in Fig. 3.

Concrete specimens were placed inside a high-efficiency thermal insulation chamber, where a high-temperature flame was introduced from the bottom inlet to simulate rapid thermal exposure conditions (Fig. 3a and d). The flame was generated through controlled combustion of liquid natural gas supplied via a dedicated gas tube. Excess hot gases were discharged through air outlets located on the sidewalls, allowing stable internal airflow conditions to be maintained throughout the heating process (Fig. 3e).

The temperature within the chamber was continuously monitored using thermocouples positioned near the specimen surfaces to ensure accurate control and recording of the thermal exposure history. Specimens were exposed to elevated temperatures following a predefined temperature–time profile, consisting of a rapid heating stage followed by a sustained holding period at the target temperature, as shown in Fig. 3b and c. This thermal regime was designed to replicate severe heat exposure conditions associated with fire

or extreme thermal environments. Upon completion of the heating stage, the gas supply was shut off and specimens were allowed to cool naturally inside the chamber. This cooling procedure was adopted to minimize thermal shock and to better represent post-fire cooling conditions in real structural scenarios.

(a) On-site configuration of the liquid natural gas–fueled heating system and testing apparatus

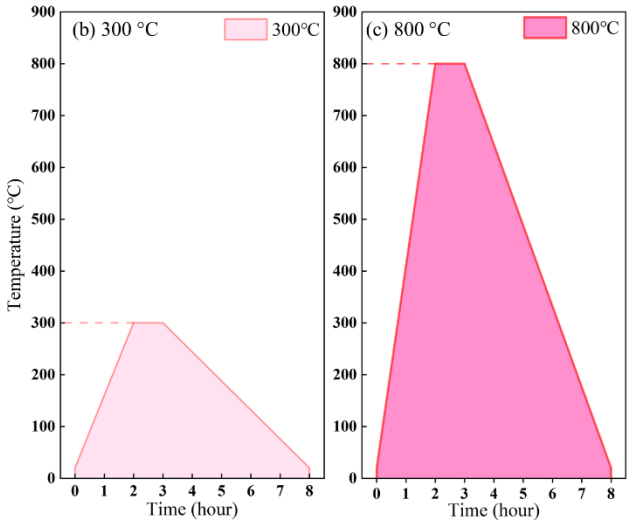

Representative temperature–time profiles applied during high-temperature exposure at: (b) 300 °C and (c) 800 °C

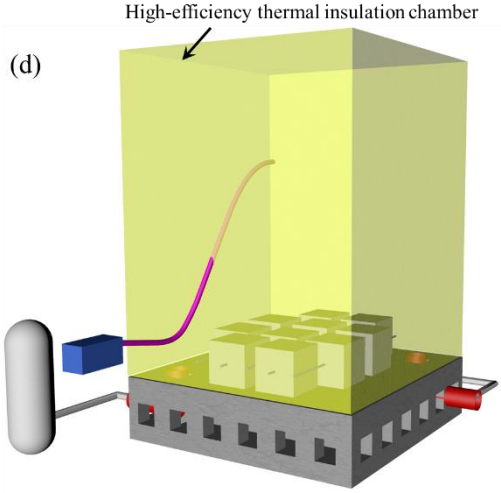

(d) Schematic illustration of the thermal exposure setup

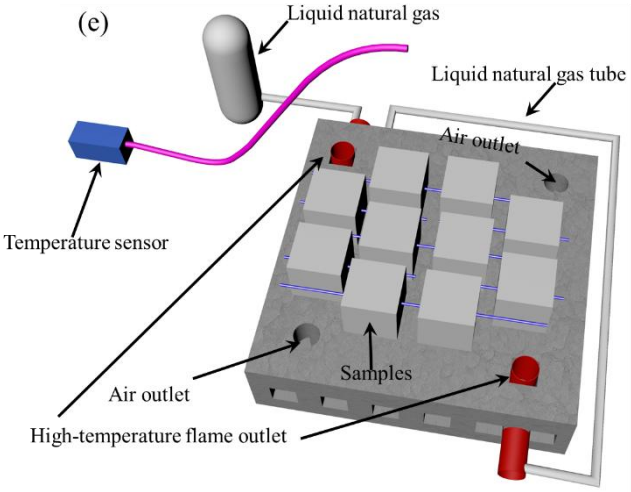

(e) Detailed schematic of the heating system.

Fig. 3. Experimental setup of the high-temperature thermal exposure process.

3.1.4 Pull-Out Testing and Data Acquisition

Pull-out tests were performed using a universal testing machine under displacement-controlled loading, as schematically illustrated in Fig. 4. Each specimen was mounted in a custom-designed loading frame to ensure accurate axial alignment between the embedded reinforcing bar and the applied tensile load (Fig. 4 a, b and d). This configuration minimized eccentric loading and ensured that the measured response was governed primarily by steel–concrete bond behavior.

(a) Photograph of the universal testing machine with the pull-out specimen

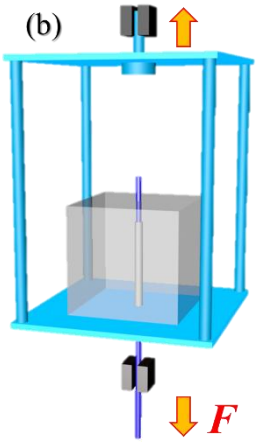

(b) schematic view of the loading frame and specimen configuration

(c) Representative concrete specimens and extracted reinforcing bars after testing

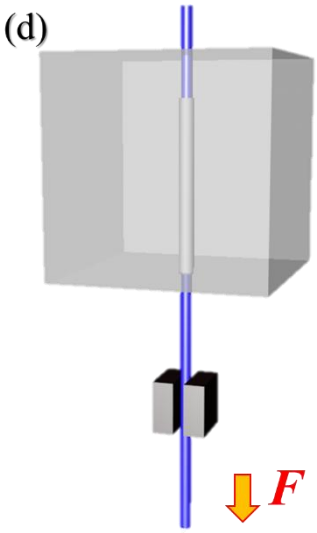

(d) Simplified representation of the pull-out test principle

Fig. 4. Pull-out test setup and post-test specimens

A monotonic displacement was applied to the reinforcing bar at a constant loading rate, inducing progressive bond slip at the steel–concrete interface. The applied load and the corresponding slip of the reinforcing bar were continuously recorded throughout the test, allowing complete load–slip responses to be obtained for each specimen. Slip was defined as the relative displacement between the reinforcing bar and the concrete surface.

Testing was continued until bond failure or pronounced post-peak degradation was observed, ensuring that both peak resistance and post-peak behavior were captured. For each corrosion–temperature combination, multiple replicate specimens were tested to ensure repeatability and to support subsequent statistical analysis. Following testing, both the concrete specimens and the extracted reinforcing bars were

visually inspected to document failure modes, interfacial damage, and surface conditions (Fig. 4c).

3.1.5 Bond Performance Indicator

Raw load–slip datasets were systematically reviewed to identify responses that were mechanically consistent with steel–concrete bond behavior. As illustrated in Fig. 4, physically meaningful pull-out responses are characterized by a nonlinear ascending branch followed by a clearly identifiable peak load. Two valid post-peak response types were observed: ductile responses, exhibiting gradual post-peak softening, and brittle responses, exhibiting an abrupt load drop immediately after the peak with minimal post-peak slip. Load–slip responses that did not exhibit these characteristics were classified as non-physical and excluded from further analysis. Such responses included near-linear load–slip relationships, absence of a distinct peak load, or lack of any discernible bond failure process. These behaviors are typically associated with instrumentation issues, incomplete loading, or data acquisition artifacts rather than true bond mechanisms.

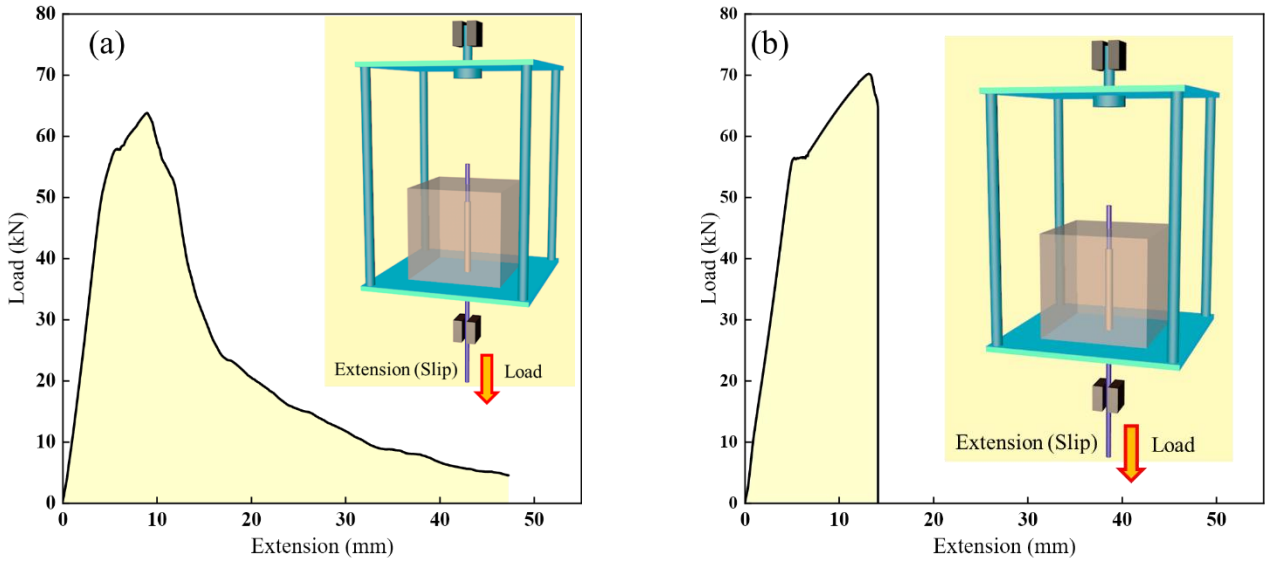

(a) Nonlinear ascending behavior with ductile post-peak responses

(b) Nonlinear ascending behavior with brittle post-peak responses

Fig. 5. Definition of mechanically meaningful load–slip responses

To ensure consistency and repeatability across the experimental database, a reproducible data screening procedure was applied to all load–slip curves. Curves exhibiting either ductile or brittle responses, as defined in Fig. 5, were retained provided that a nonlinear ascending branch and a well-defined peak load were present. This data quality control step ensured a mechanically meaningful and statistically reliable dataset suitable for project-level interpretation and modeling. The peak pull-out load, defined as the maximum load attained on the load–slip curve (Fig. 5), was selected as the primary quantitative indicator of steel–concrete bond performance. This parameter represents the maximum

mobilized interfacial resistance between the reinforcing steel and concrete and marks the onset of bond-controlled failure, regardless of whether the subsequent response is ductile or brittle. For each corrosion–temperature condition, the mean value and standard deviation of the peak pull-out load were calculated from the screened dataset, providing measures of both central tendency and variability required for comparative analysis and subsequent probabilistic modeling.

3.1.6 Experimental Matrix and Scope

The combined experimental matrix consisted of two concrete systems (PLC and GPC), four corrosion states, and three thermal exposure conditions. This design enables systematic evaluation of individual and coupled effects of corrosion severity and temperature on steel–concrete bond behavior, while maintaining a manageable and reproducible test program consistent with the objectives of the TriDurLE project.

3.2 Robust, Dynamic, and Adaptive Decision Framework

This section presents the integrated methodology developed to assess and enhance the long-term fire performance of RC bridges in chloride-laden environments under deep uncertainty. The methodology combines two complementary components: (1) a robustness-based material evaluation using IGDT and (2) a dynamic adaptive planning model that supports the timing of interventions. Together, these methods provide a structured framework for identifying robust materials and implementing adaptive maintenance strategies across an infrastructure system's life cycle.

3.2.1 Implementation of Info-Gap Decision Theory

In the early stages of infrastructure design and planning, uncertainty manifests across a spectrum, from relatively well-understood conditions to entirely unknown or unknown futures. Often, critical information regarding environmental exposures, the properties of new material, or long-term deterioration mechanisms remains incomplete or vague. In this analysis, we deliberately avoid making unwarranted assumptions or assigning specific probability distributions or membership functions to uncertain parameters. Even when interval estimates are defined, these bounds may later prove inadequate, as new data becomes available or unexpected conditions occur, which are beyond the initial expectations.

To accommodate this pervasive uncertainty, each variable is treated as having a range of indeterminate size. This modeling approach allows for flexible deviation from nominal values and avoids overconfidence in parameter estimates. Conceptually, this leads to the formation of n-dimensional hypercubes (as illustrated in Fig. 6a), each representing a multidimensional space of plausible variations in uncertain variables. These hypercubes reflect the intricate and often interdependent nature of deep uncertainty affecting infrastructure systems. The formulation for generating deeply uncertain variables is

adopted from Marchau et al. [36] and is given by:

$$U(h) = \{x = (x_k)_{1\le k\le n} : hw_k^{lower} \le x_k - x_k^{(0)} \le hw_k^{upper}\} \quad \text{Eq. 3}$$

where $U(h)$ = the information gap (IG) model of uncertainty; h = the horizon of uncertainty; w_k^{lower} and w_k^{upper} = the scaling coefficients; $x = (x_k)_{1\le k\le n}$ = the n number of uncertain variables, $x_k^{(0)}$ = the nominal value of the uncertain variable x_k; and $U(h)$ = the envelope-bound IG model. Here, $U(h)$ is not a single set, but rather an unbounded family of nested sets (hypercubes). The hypercubes grow as h gets larger, as shown in Fig. 6b. The scaling coefficients, w_k^{lower} and w_k^{upper}, are the sets such that the assumed ranges are recovered when $h = 1$. This formulation serves as the foundation for IGDT, which is designed to evaluate the performance of decisions across the space defined by the uncertainty sets. The envelope-bound IG model constrains the uncertain deviations to an expandable envelope while being more flexible than other IG models. This is because they can be used to represent a wider range of uncertainty types, including both quantitative and qualitative uncertainty. For example, other IG models, such as Fourier-bound models, are useful when we can express an uncertain function as a Fourier series. As we have multiple random variables interconnected by probabilistic relationships, the envelope-bound IG model becomes particularly valuable. Probabilistic relationships imply dependencies between variables, and capturing these dependencies is crucial for robust decision-making. Each random variable x_i in the system is associated with an uncertainty set defined by an envelope bound as:

$$U_i(h)=[x_i^{(0)} + hw_i^{lower}, x_i^{(0)} + hw_i^{upper}] \quad \text{Eq. 4}$$

When there are probabilistic relationships between x_i and x_j (e.g., $x_j = f(x_i)$), the uncertainty set for x_j must reflect this dependence. Let's consider a simple linear relationship between two random variables x_i and x_j.

$$x_j = ax_i + b \quad \text{Eq. 5}$$

where a and b = the constants. To capture this interdependency in the uncertainty sets, we can adjust the uncertainty set for x_j based on the uncertainty set of x_i as follows

$$U_j(h)=[ax_i^{(0)} + b + hw_j^{lower}, ax_i^{(0)} + \mathrm{b} + hw_j^{upper}] \quad \text{Eq. 6}$$

This representation allows for a more comprehensive exploration of uncertainties, considering both the individual parameter uncertainties and their interdependencies. After generating deeply uncertain random variables, we can use them to analyze the performance of the system. Then, the question we wish

to answer is whether the performance remains requirement-compliant if real-world conditions to which the bridge/system might be subjected deviate from those assumed in the simulation. More specifically, we want to estimate the greatest horizon of uncertainty, $\hat{h}$, up to which the predicted maximum performance does not violate the critical requirement for all realizations of the uncertain variables in the IG model illustrated in Equation 1. This can be mathematically stated as [36]:

$$\hat{h}(y_{critical}) = \max_{\{h \geq 0\}} \left(\max_{\{x \epsilon\, U(h)\}} y_{max}(x) \leq y_{critical} \right) \quad \text{Eq. 7}$$

where $\hat{h}$ = the robustness or the greatest horizon of the uncertainty of the system given a performance requirement, $y_{critical}$; y_{max} = the predicted maximum performance of the system. For example, if $\hat{h} = 0.4$, then it means that the design satisfies the performance requirement as long as none of the uncertain variables *x* deviates from its nominal value by more than 40%. We can also define it as the performance is guaranteed to satisfy the critical performance criterion as long as real-world conditions do not deviate from nominal settings of the simulation by more than 40%. This concludes the process of estimating the robustness measure using IDGT. The results of this analysis guide material selection and act as input into the adaptive decision-making model described in the following section.

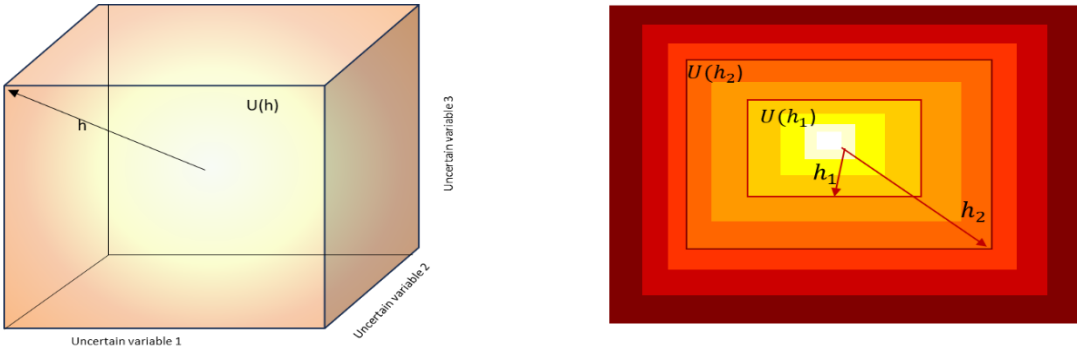

Fig. 6. (a) 3-dimensional hypercube and (b) horizon of uncertainty in info-gap theory

3.2.2 Dynamic adaptive decision planning model

IGDT is designed to address deep uncertainty by providing a robustness-centered approach to decision-making. In this study, two types of RC are evaluated: PLC and GPC. GPC has gained attention for its improved fire resistance and sustainability; however, substantial uncertainties surrounding its long-term behavior persist due to its relatively recent development [37-39]. In this context, IGDT is used to determine which concrete type offers higher fire resistance and greater robustness across a wide range of uncertain future conditions.

Considering robustness during material selection is essential to ensure consistent performance under varying and unforeseen scenarios. A robust concrete type is one that maintains acceptable structural performance, even when external variables, such as deterioration rates or environmental stressors, deviate significantly from assumed conditions.

While IGDT supports robust initial decision-making, it typically offers static guidance based on a single decision point in time. In contrast, DAPP introduces a temporal dimension to the decision-making process, recognizing that infrastructure decisions may need to evolve in response to emerging information, shifting scenarios, or changing constraints. The integration of IGDT with DAPP provides a comprehensive framework: IGDT is used to identify robust initial decisions, and DAPP facilitates flexibility and adaptability as new information becomes available over time.

DAPP is a recognized Decision Making under Deep Uncertainty (DMDU) approach that explicitly incorporates time-dependent decision points. It explores multiple adaptation pathways—sequences of decision options under different plausible futures—and highlights path dependency, which refers to how early decisions can constrain or expand future options. Combining DAPP with IGDT yields a powerful hybrid strategy for long-term, uncertainty-informed infrastructure planning.

In this study, deeply uncertain parameters are generated using the IGDT framework, while DAPP is modified to support more flexible adaptation planning. Scenario planning within the DAPP structure includes representative futures such as no climate change, low emissions, and high emissions trajectories.

The first step in the dynamic adaptive process is to evaluate fire performance-enhancing strategies. We formulate an optimization model with the objective of minimizing the average cost of interventions over time, while ensuring that fire performance and reliability criteria are satisfied. The optimization problem is expressed as:

$$\text{Minimize} \quad C_{avg} \qquad \text{Eq.8}$$

$$\text{Constraints:} \quad C_i \leq C_{max}$$

$$F_i \geq F_{min}$$

$$r_i \leq r_{max}$$

where C_{avg} = the average cost of the fire performance-enhancing strategy; C_i = the cost of fire performance-enhancing strategy i; F_i = the fire performance of fire performance-enhancing strategy i; r_i = the structural reliability of fire performance-enhancing strategy i; C_{max} = the maximum allowable cost; F_{min} = the minimum allowable fire performance; and r_{max} = the maximum allowable structural reliability.

It is identified as a literature gap that, in many studies, the decision horizon and forecast horizon are chosen based on expert knowledge, but this can lead to uncertainty. The use of fixed or time-constant horizons may oversimplify the decision-making process and fail to capture the complexities and uncertainties inherent in dynamic systems. We consider robustness as a measure for choosing the forecast horizon. Robustness helps us understand the limit of uncertainty when choosing the forecast horizon. Along with the robustness measure, we can also consider parameter constraints and the accuracy of forecasting methods in choosing the forecast horizon. We forecast uncertain parameters related to climate change, the deterioration process, etc. For example, chloride-induced corrosion in reinforced concrete can be modeled using tools such as Life-365, which provide service life predictions under various environmental and exposure conditions. These tools may support the selection of parameter ranges and deterioration rates used in adaptive planning. For this forecast, we estimate the robustness, check for parameter constraints, estimate the accuracy of the forecasting method, and choose the forecast horizon. For deeply uncertain parameters, it is crucial to ensure that their forecasted values do not exceed their acceptable limits. This can be expressed as follows:

$$p_{min} \leq p_f \leq p_{max} \quad \text{Eq. 9}$$

where p_{min} = the minimum acceptable value of the parameter; p_f = the forecasted value of the parameter; and p_{max} = the maximum acceptable value of the parameter. The overall equation for estimating the forecast horizon, considering robustness, parameter constraints, and forecasting method accuracy, can be written as follows:

$$\text{Forecast horizon} = \min (h_{min}, h_r, h_{acc}) \quad \text{Eq. 10}$$

where h_{min} = the minimum forecast horizon based on parameter constraints; h_r = the forecast horizon based on the robustness measure; and h_{acc} = the forecast horizon based on forecasting method accuracy.

The next step in the methodology is to choose the decision horizon. So, in this work, we consider fire performance, policy changes, new technology, and the cost of maintenance action as criteria to choose the next decision point. Let F_t represent the fire performance of the bridge at time t. The fire performance F_t is a function of uncertain parameters concerning material properties (U_m), uncertain parameters concerning climate change (U_{cc}), uncertain parameters concerning socio-economic changes(U_{se}), and fire resistance of concrete (f_r). Here, fire resistance can be affected by any fire-enhancing strategy that we apply.

$$F_t = \text{function} (U_m, U_{cc}, U_{se}, .., f_r) \quad \text{Eq. 11}$$

The decision horizon can be determined by setting a threshold for acceptable fire performance, F_{min}. If the forecasted fire performance at any time t falls below F_{min}, the decision horizon is reached. Let P_t represents the impact of policy changes on the fire performance of the bridge at time t. Policy changes can affect fire performance by introducing new regulations, safety standards, or technologies related to bridge construction and fire safety. The decision horizon can be adjusted based on the forecasted impact of policy changes. Let B_t represents the available budget for bridge maintenance and fire safety improvements at time t. The decision horizon can be limited by the available budget. If the forecasted costs of maintaining acceptable fire performance exceed the available budget, the decision horizon is reached. Let T_t represents the impact of new technologies on the fire performance of the bridge at time t. New technologies can improve fire performance by introducing fire-resistant materials, construction techniques, or monitoring technologies. The decision horizon can be extended based on the forecasted impact of new technologies. The overall equation for deciding on the decision horizon, considering fire performance, policy changes, budget, and new technologies and forecast horizon F_h, can be expressed as:

$$\text{Decision horizon} = (t \mid \min(F_t < F_{min},\ F_t + P_t < F_{min},\ C_t > B_t,\ F_t + T_t < F_{min}, F_h)) \quad \text{Eq. 12}$$

This equation ensures that the decision horizon is based on all relevant factors and that the bridge is maintained in a safe condition with acceptable fire performance.

Chapter 4. Results and Discussion

This chapter presents and discusses the experimental results obtained from pull-out testing of reinforced concrete specimens subjected to combined corrosion and thermal exposure. The results are organized to systematically examine (a) electrochemical characterization of corrosion states, (b) steel–concrete bond response under different corrosion and temperature conditions, and (c) comparative performance of Portland limestone cement concrete (PLC) and geopolymer concrete (GPC). Emphasis is placed on identifying trends, interaction effects, and degradation patterns relevant to TriDurLE Objective 1, while providing a quantitative basis for subsequent probabilistic and life-cycle assessment under Objective 2. At the end of this chapter, we will introduce a simple conceptual example to show how the experimental results can be used in the proposed decision framework.

4.1 Electrochemical Characterization of Corrosion States

Electrochemical characterization was performed to quantify corrosion activity corresponding to the four corrosion states defined in Section 3.1.3. The evolution of OCP and CCD with increasing conditioning duration is summarized in Table 2. Mean values and standard deviations were calculated based on specimen-level paired OCP and LPR measurements.

As shown in Fig. 7, the mean OCP exhibited a pronounced shift toward more negative values upon corrosion conditioning. The unconditioned specimens (0 day) displayed relatively noble OCP values, with a mean of approximately −255 mV (vs. reference), indicative of predominantly passive steel conditions. After 3 days of chloride exposure, the mean OCP decreased substantially to approximately −720 mV, reflecting depassivation and the onset of active corrosion. With further conditioning, the mean OCP did not follow a strictly monotonic trend. Specimens conditioned for 6 days exhibited a less negative mean OCP (approximately −659 mV) compared to the 3-day condition, while the 9-day specimens showed a further shift toward more noble potentials (approximately −533 mV). In addition, the standard deviation of OCP increased markedly with conditioning duration, reaching values exceeding 100 mV for the 6-day and 9-day conditions.

This non-monotonic evolution and increased scatter in OCP are consistent with the localized nature of chloride-induced corrosion in concrete. As corrosion progresses, the formation of corrosion products and partial blockage of anodic sites can locally alter electrochemical conditions, leading to apparent ennoblement of measured OCP despite ongoing corrosion activity. Therefore, OCP alone does not provide a unique or monotonic indicator of corrosion severity at advanced stages.

In contrast to OCP, the corrosion current density derived from LPR measurements exhibited a clearer

increase in corrosion activity with conditioning duration. The unconditioned specimens showed negligible corrosion current density, on the order of 10^{-6} A/cm^2, consistent with passive steel behavior. Following 3 days of conditioning, CCD increased by nearly two orders of magnitude, indicating the establishment of active corrosion processes. Specimens conditioned for 6 days exhibited a comparable level of corrosion current density to the 3-day condition, with overlapping mean values and substantial scatter. This plateau behavior suggests that corrosion activity had become spatially localized, with competing effects of anodic dissolution and corrosion product accumulation influencing the measured polarization response. After 9 days of conditioning, the mean corrosion current density increased further to approximately 4.7×10^{-4} A/cm2, indicating intensified corrosion activity despite the concurrent partial recovery of OCP toward less negative values. The divergence between OCP and CCD trends highlights the limitation of relying on a single electrochemical parameter to characterize corrosion severity. While OCP reflects the thermodynamic tendency for corrosion, CCD provides a more direct measure of corrosion rate and remained elevated for specimens classified as medium and severe corrosion. The combined OCP–CCD response confirms that corrosion progression in chloride-exposed reinforced concrete is non-uniform and non-monotonic when assessed using individual electrochemical indicators. Consequently, corrosion states in this study were classified based on the combined interpretation of OCP and corrosion current density, rather than on conditioning duration or OCP thresholds alone. This approach ensures consistency between measured electrochemical activity and the corrosion severity categories used in subsequent mechanical and thermal performance analyses.

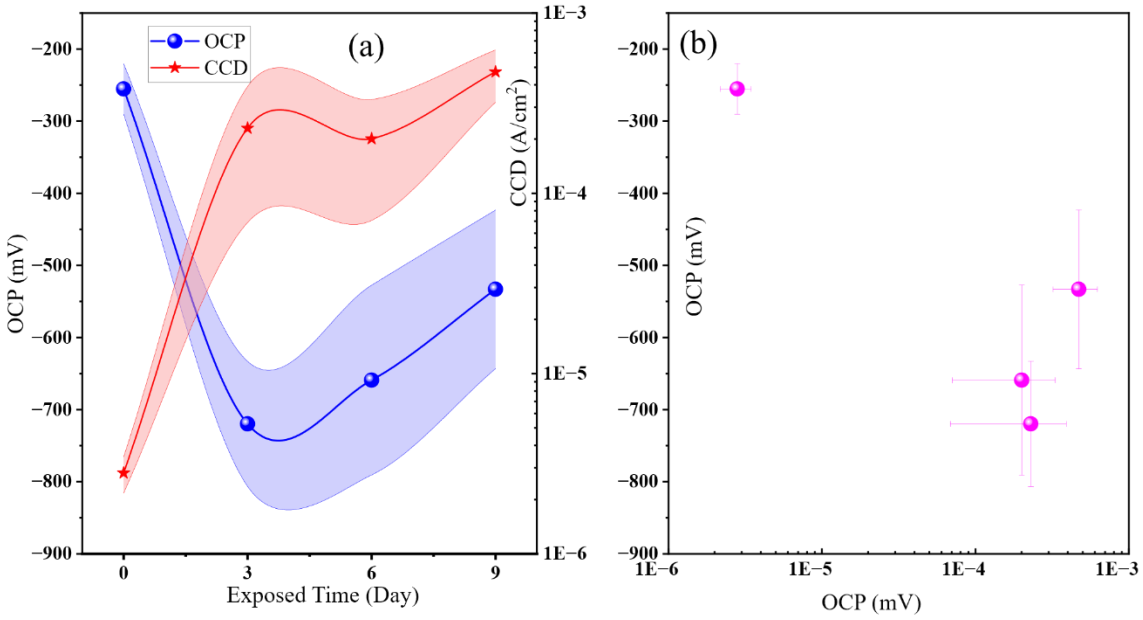

Fig. 7. Electrochemical characterization of corrosion progression

4.2 Load–Slip Curve Characteristics

Cleaned load–slip curves obtained from pull-out tests under all corrosion states and thermal exposure conditions exhibit physically meaningful steel–concrete bond responses. The curves are characterized by nonlinear ascending branches, clearly identifiable peak loads, and post-peak degradation behavior, consistent with the bond response classification defined in Section 3. Both ductile responses, marked by gradual post-peak softening, and brittle responses, characterized by abrupt post-peak load drops, are observed across the test matrix. Clear material-dependent differences are evident in both peak formation and post-peak behavior. For PLC specimens, post-peak load reduction is generally steeper, particularly under elevated temperature exposure, indicating a more brittle bond degradation process. In contrast, GPC specimens tend to exhibit smoother post-peak degradation and reduced scatter among replicate tests, reflecting a more stable bond response. These material-dependent trends are consistently observed across corrosion levels and become increasingly pronounced with rising exposure temperature. Figs. 8-11 present the cleaned load–slip curves for PLC and GPC specimens under different corrosion states and thermal exposure conditions, illustrating the combined effects of corrosion severity, temperature, and binder type on steel–concrete bond behavior.

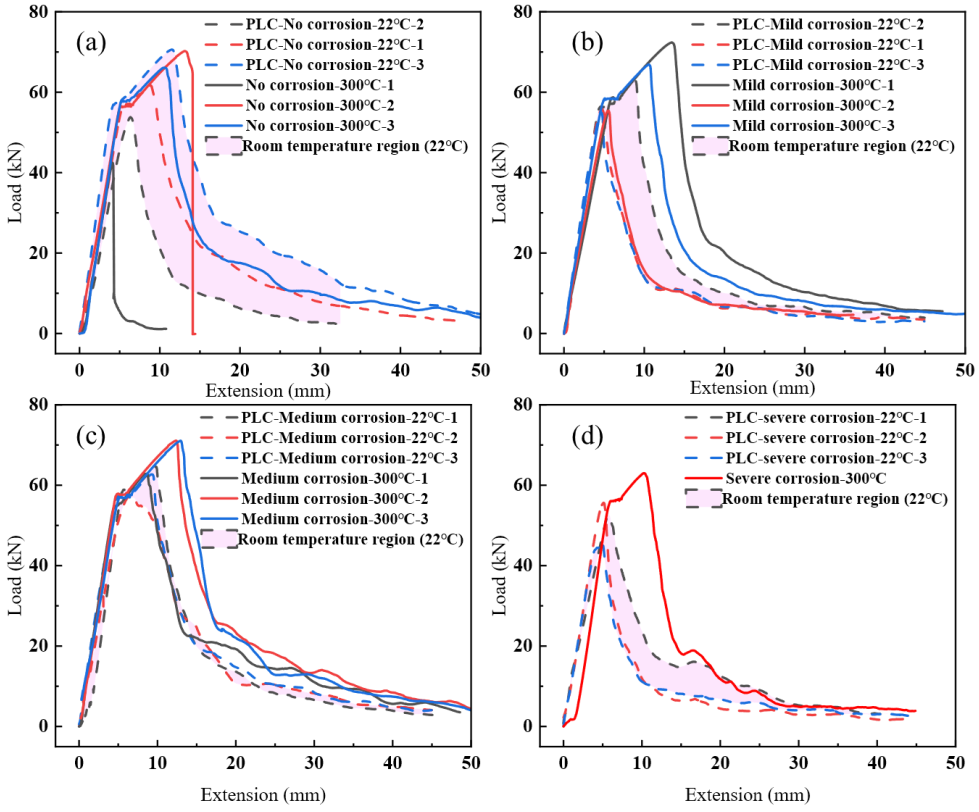

Fig. 8 PLC specimens' load–slip curves at room temperature vs. 300 °C.

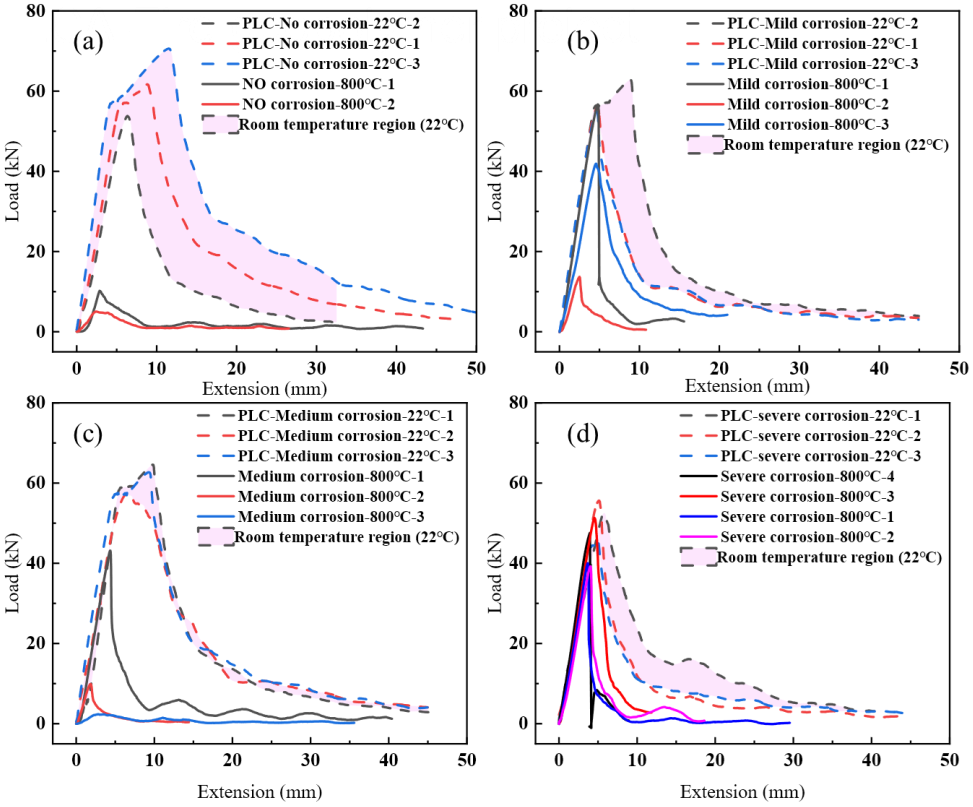

Fig. 9 PLC specimens' load–slip curves at room temperature vs. 800 °C

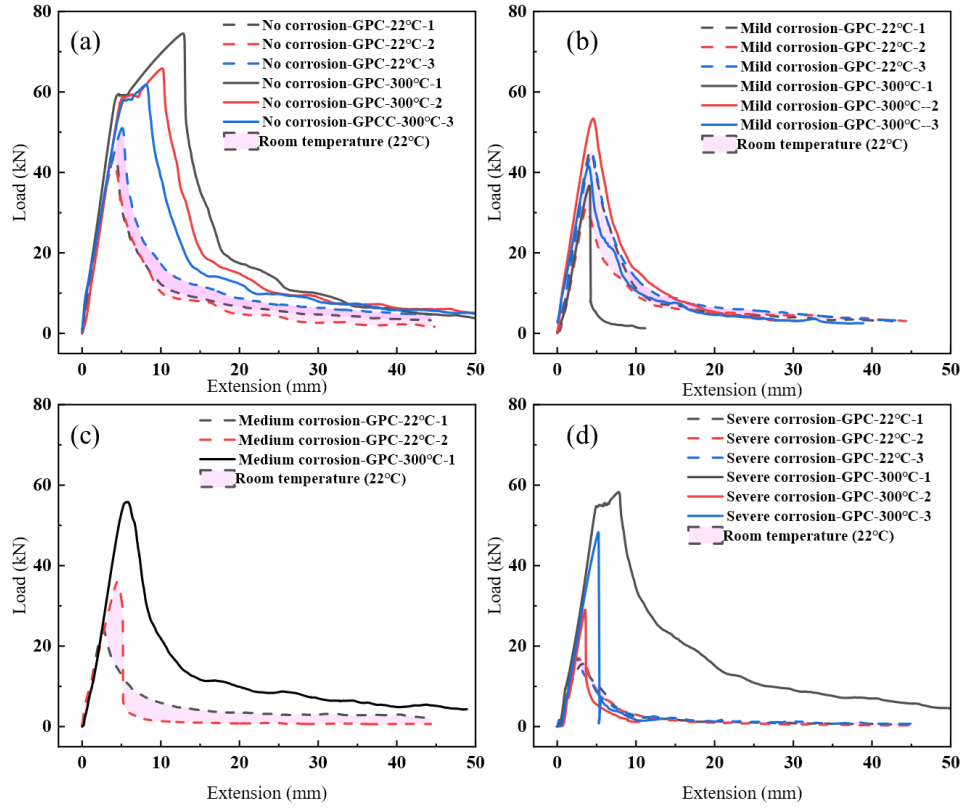

Fig. 10 GPC specimens' load–slip curves at room temperature vs. 300 °C

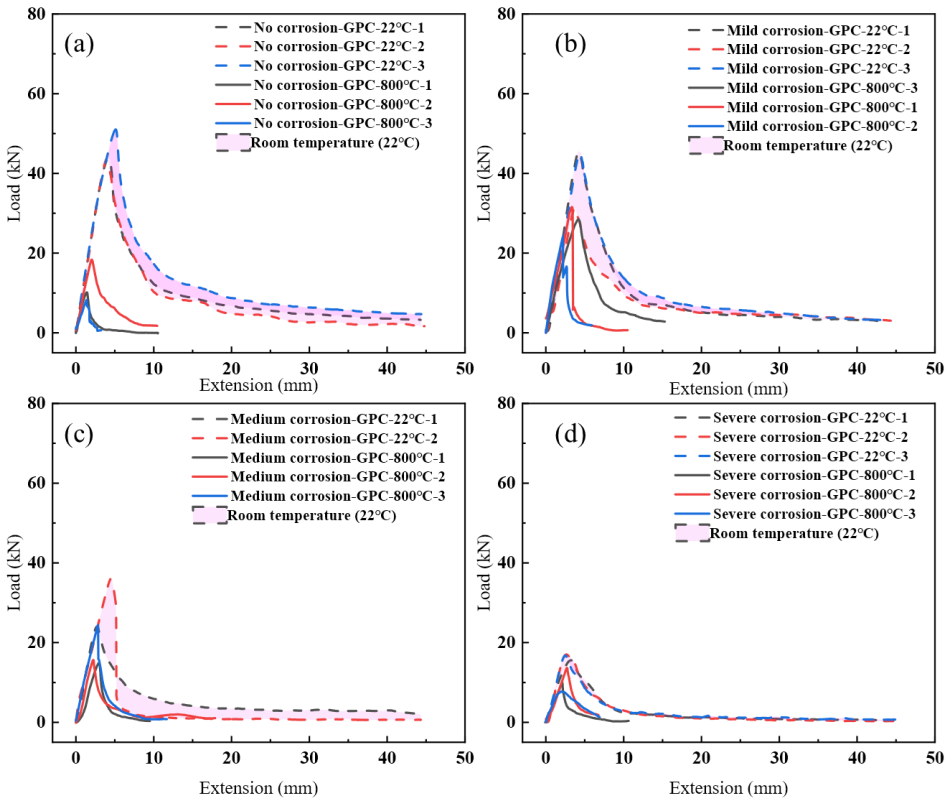

Fig. 11 GPC specimens' load–slip curves at room temperature vs. 800 °C

4.3 Effect of Corrosion and Temperature on Peak Pull-Out Load

Fig. 12 summarizes the variation of average peak pull-out load with corrosion severity and exposure temperature for both PLC and GPC specimens. Error bars represent one standard deviation calculated from replicate tests, reflecting specimen-to-specimen variability. For PLC specimens (Fig. 12a), peak pull-out load under ambient conditions remains relatively high across corrosion levels. Mild and medium corrosion exhibit comparable, or in some cases slightly higher, peak values than the uncorroded condition. At an exposure temperature of 300 °C, the peak pull-out load generally remains at a level similar to that observed under ambient conditions, indicating limited degradation of bond capacity at moderate temperature. In contrast, exposure to 800 °C results in a pronounced reduction in peak pull-out load for all corrosion levels. Moreover, the extent of bond degradation increases systematically with corrosion severity, with severely corroded specimens exhibiting the lowest residual bond capacity.

For GPC specimens (Fig. 12b), peak pull-out load decreases more consistently with increasing corrosion severity across all temperature levels. Under ambient conditions, corrosion leads to a progressive reduction in bond capacity. At 300 °C, uncorroded and mildly corroded specimens retain a

substantial portion of their peak pull-out load, whereas medium and severe corrosion result in noticeably lower values. Exposure to 800 °C causes a substantial reduction in peak pull-out load for all corrosion levels, with severe corrosion corresponding to the lowest residual bond capacity among all test conditions. The scatter in peak pull-out load, as indicated by the error bars, increases with both exposure temperature and corrosion severity. This trend reflects the growing heterogeneity of steel–concrete bond behavior under combined thermal and corrosion-induced damage and highlights the strong interaction between corrosion state and temperature in governing residual bond performance.

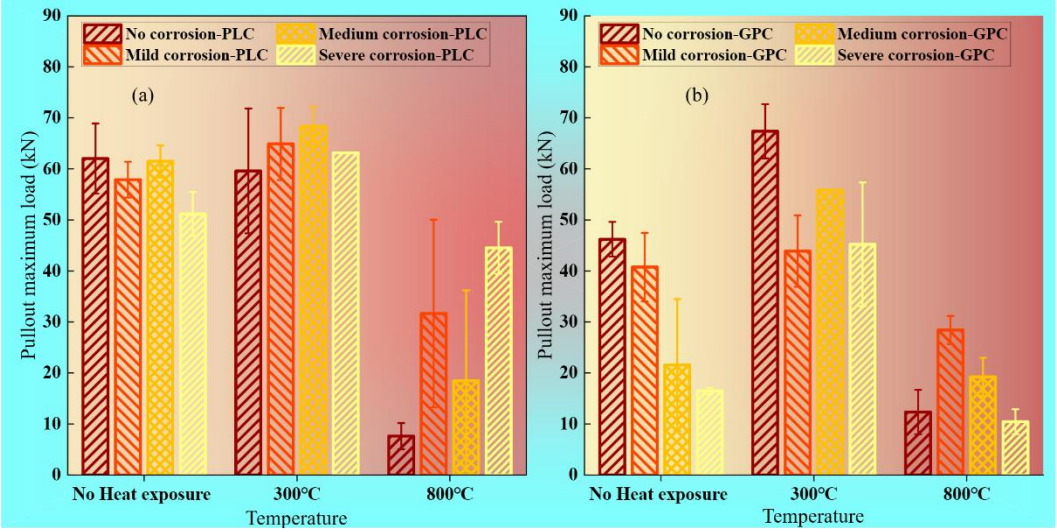

Fig. 12 Peak pull-out load of PLC and GPC specimens under varying conditions

4.4 Comparative Performance of PLC and GPC

For PLC specimens, the effect of corrosion severity on peak pull-out load is strongly dependent on exposure temperature. Under ambient conditions, mild and medium corrosion exhibit comparable or even higher average peak pull-out loads than the uncorroded condition. A similar trend is observed at 300 °C, where mild and medium corrosion result in higher average peak loads (approximately 65–68 kN) than the no-corrosion case (approximately 60 kN). This behavior indicates that limited corrosion may locally enhance mechanical interlock and confinement at the steel–concrete interface prior to the onset of severe thermal damage. In contrast, exposure to 800 °C leads to a pronounced reduction in peak pull-out load across all corrosion levels. Although bond degradation generally intensifies with increasing corrosion severity, the response remains non-monotonic. Medium corrosion exhibits the lowest average peak load at 800 °C (approximately 18 kN), while severe corrosion shows a slightly higher residual capacity (approximately 45 kN), accompanied by substantial scatter. These results highlight a strong interaction

between corrosion-induced interfacial modification and temperature-induced matrix degradation, resulting in complex and non-linear bond deterioration behavior in PLC specimens.

For GPC specimens, peak pull-out load exhibits a more consistent reduction with increasing corrosion severity across all temperature levels. Under ambient conditions, corrosion generally leads to a decrease in average bond capacity, with medium and severe corrosion showing significantly lower peak loads than the uncorroded condition. At 300 °C, no enhancement in peak pull-out load is observed; instead, corrosion severity remains the dominant factor governing bond degradation. Exposure to 800 °C results in substantial bond capacity loss for all corrosion states, with average peak pull-out loads generally below 20 kN. Although some scatter is present, the relative ordering of corrosion severity is largely preserved, indicating a more predictable degradation pathway. Compared to PLC, GPC specimens exhibit reduced variability and a more monotonic response to combined corrosion and thermal exposure.

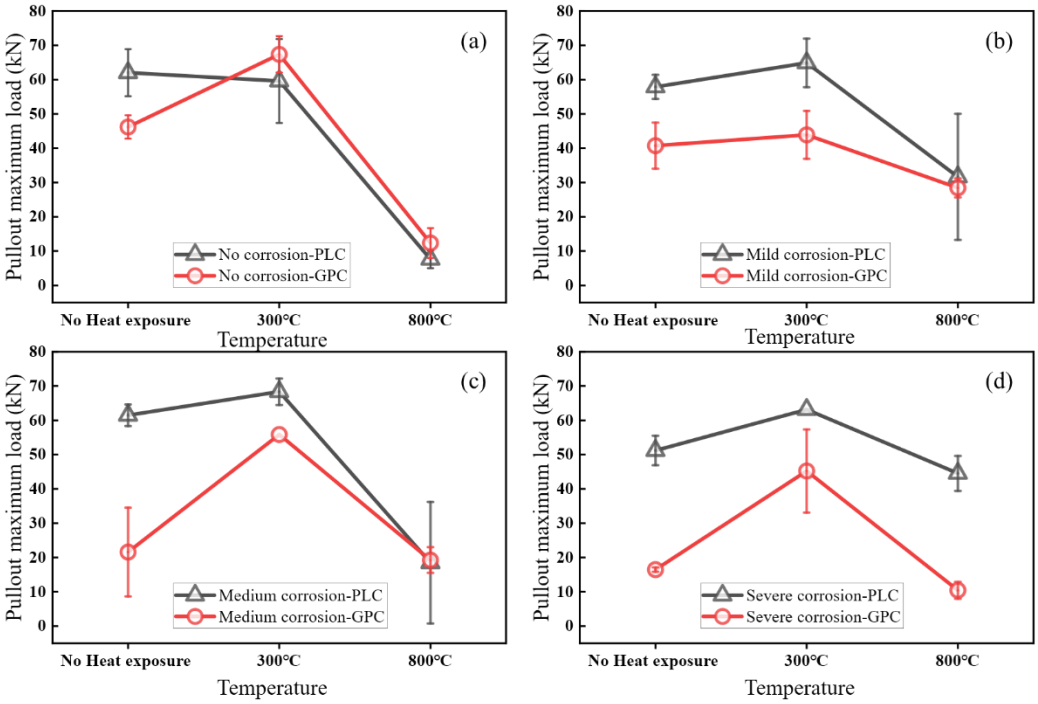

Fig. 13. PLC and GPC's peak pull-out load trends for under varying conditions

A direct comparison of PLC and GPC specimens under coupled corrosion and thermal exposure, based on the summary statistics in Table. 3 and the temperature-dependent trends in Fig. 13, reveals distinct material-dependent bond degradation patterns. At low or no corrosion levels under ambient conditions, the average peak pull-out loads of PLC and GPC are generally comparable, with PLC exhibiting slightly higher mean values in some cases. At 300 °C, both materials retain a substantial fraction of their bond capacity; however, GPC demonstrates more consistent performance across corrosion levels, whereas PLC

exhibits greater scatter. At 800 °C, a clear divergence in bond performance emerges: GPC retains a higher fraction of its peak pull-out load than PLC across all corrosion levels, with the difference becoming increasingly pronounced under medium and severe corrosion conditions. In contrast, PLC experiences a sharper reduction in peak pull-out load accompanied by increased variability. Collectively, these results demonstrate distinct material-dependent trends in steel–concrete bond degradation under combined corrosion and thermal exposure and provide a quantitative basis for the comparative analysis developed in the subsequent Discussion section.

Table. 3 PLC and GPC peak pull-out load for specimens under different conditions

Conditions		PLC			GPC		
Corrosion conditioning	Temperature	Pullout maximum load (kN)	Average value (kN)	Standard deviation (kN)	Pullout maximum load (kN)	Average value (kN)	Standard deviation (kN)
No corrosion	No heat exposure(Room temperature)	53.81	62.03	6.86	43.95	46.21	3.41
		70.60			43.64		
		61.69			51.03		
	300ºC	42.46	59.60	12.24	65.86	67.38	5.32
		70.23			74.52		
		66.11			61.77		
	800ºC	10.20	7.62	2.58	8.21	12.35	4.36
		5.04			18.38		
		-			10.45		
Mild corrosion	No heat exposure(Room temperature)	62.83	57.88	3.52	45.33	40.75	6.71
		54.94			45.67		
		55.88			31.26		
	300ºC	72.37	64.89	7.07	53.38	43.88	6.99
		66.90			36.74		
		55.40			41.53		
	800ºC	41.91	31.66	18.40	24.07	28.44	2.75
		13.69			29.64		
		14.34			28.47		
		56.68			31.56		
Medium corrosion	No heat exposure(Room temperature)	57.17	61.48	3.15	4.69	21.58	12.91
		64.59			36.04		
		62.69			24.02		
	300ºC	62.88	68.34	3.86	55.85	55.85	0.00
		71.07			-		
		71.08			-		
	800ºC	43.16	18.47	17.73	15.64	19.25	3.73
		9.90			24.38		
		2.36			17.72		
Severe corrosion	No heat exposure(Roo	52.58	51.18	4.32	15.58	16.48	0.64
		55.63			17.06		

	m temperature)	45.34			16.79		
	300ºC	63.16	63.16	0.00	29.06	45.22	12.13
		-			48.32		
		-			58.28		
	800ºC	47.58	44.53	5.09	9.94	10.44	2.45
		51.31			7.72		
		39.22			13.66		
		40.02					

The experimental results obtained in this study are broadly consistent with mainstream findings reported for reinforced concrete systems subjected to elevated temperatures and corrosion. Previous studies have demonstrated that steel–concrete bond strength decreases significantly with increasing temperature due to degradation of the cementitious matrix, thermal incompatibility between steel and concrete, and progressive loss of confinement [16, 26]. Similar temperature-dependent degradation trends have also been reported for geopolymer-based systems, in which bond-related properties generally remain stable up to moderate temperatures (approximately 200–300 °C) but deteriorate rapidly at higher temperature levels [40].

The present results confirm these general observations for both PLC and GPC specimens. In particular, the pronounced reduction in peak pull-out load observed at 800 °C aligns well with high-temperature bond degradation thresholds reported in the literature for both conventional and alternative cementitious systems. Importantly, by explicitly incorporating corrosion conditioning, the present study extends prior temperature-only investigations and demonstrates that pre-existing corrosion damage significantly alters the temperature sensitivity of steel–concrete bond performance. This finding highlights the limitation of extrapolating bond degradation trends derived from uncorroded specimens to aging reinforced concrete infrastructure exposed to chloride environments.

4.5 Quantitative Degradation Trends and Project-Level Interpretation

Quantitative analysis of peak pull-out load indicates that both corrosion and temperature contribute substantially to steel–concrete bond degradation, with a clear and non-negligible coupling effect. The normalized peak pull-out loads are summarized in Table. 3, together with the comparative trends shown in Fig. 13, provide a consistent framework for evaluating this interaction across materials and exposure conditions. For PLC specimens, the effect of temperature on bond degradation is strongly dependent on corrosion severity. Uncorroded PLC specimens experience an approximately 88% reduction in peak pull-out load after exposure to 800 °C relative to the unheated condition. In contrast, under severe corrosion,

the relative peak pull-out load at 800 °C remains at approximately 0.72, corresponding to a more moderate 28% reduction relative to the unheated severe-corrosion condition. This apparent reduction in temperature sensitivity reflects a corrosion-dependent modification of bond degradation mechanisms, consistent with the non-monotonic interaction trends observed in Section 4.3. For GPC specimens, under no corrosion, exposure to 300 °C results in an approximately 46% increase in relative peak pull-out load relative to the unheated condition. This apparent increase may be attributed to further geopolymer gel condensation and moisture redistribution rather than intrinsic bond enhancement, and should therefore be interpreted as a transitional response rather than a strengthening mechanism. With further temperature increase to 800 °C, a substantial reduction in bond capacity is observed across all corrosion states, indicating that thermal damage ultimately dominates bond degradation behavior. With increasing corrosion severity, the relative peak pull-out load at 800 °C decreases progressively from approximately 0.62 under mild corrosion to approximately 0.23 under severe corrosion, corresponding to overall reductions on the order of 60–75%. Compared with PLC, GPC exhibits a more more monotonic on average degradation trend with increasing temperature and corrosion severity. These quantitative trends demonstrate that corrosion acts as a critical preconditioning factor that amplifies temperature-induced bond degradation. The results further indicate that bond reduction approaches based solely on temperature exposure may substantially underestimate bond loss in reinforced concrete systems subjected to long-term chloride-induced corrosion. From a project-level perspective, these findings underscore the necessity of incorporating coupled corrosion–temperature effects into life-cycle performance evaluation and reliability-based assessment frameworks for reinforced concrete infrastructure.

The three-dimensional response surfaces of relative maximum pull-out load for GPC and PLC, shown in Figs. 14 and 15, provide an integrated visualization of the coupled effects of corrosion severity and thermal exposure on steel–concrete bond performance. By normalizing the peak pull-out load with respect to the uncorroded, unheated reference condition, these surfaces highlight relative bond degradation or retention across the multi-hazard domain. For GPC, the response surface exhibits a smooth and continuous variation across the corrosion–temperature space. At ambient temperature and 300 °C, the relative peak pull-out load remains close to or above unity over a broad range of corrosion levels, indicating limited sensitivity to isolated corrosion or moderate thermal exposure. At 800 °C, a largely monotonic reduction in relative bond capacity is observed with increasing corrosion severity, suggesting that thermal damage dominates bond degradation, with corrosion acting primarily as an amplifying factor rather than an independent driver.

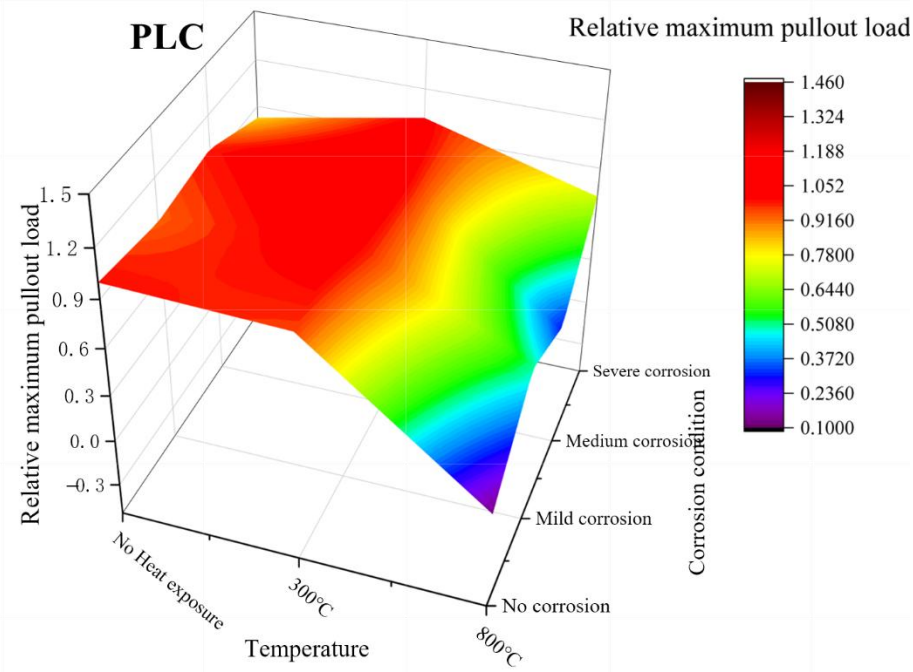

Fig. 14 Relative peak pull-out load of PLC under varying conditions

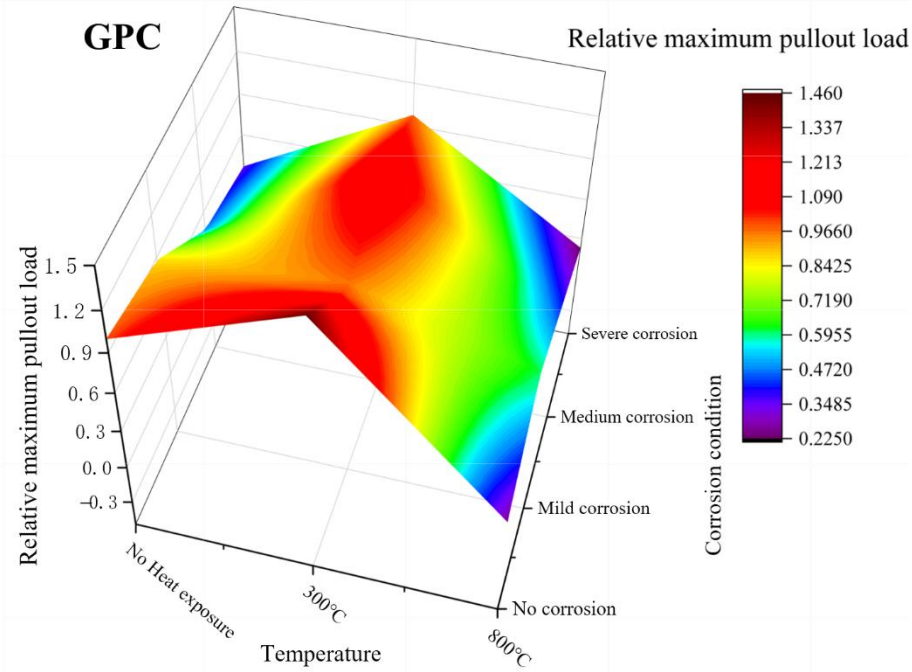

Fig. 15 Relative peak pull-out load of GPC under varying conditions

In contrast, the PLC response surface reveals a more pronounced and non-uniform interaction between corrosion and temperature. At ambient temperature and 300 °C, PLC exhibits localized regions of elevated relative peak pull-out load at low to medium corrosion levels, reflecting corrosion-induced surface roughening and temporary enhancement of frictional resistance at the steel–concrete interface. However, this apparent benefit rapidly diminishes under severe thermal exposure. At 800 °C, PLC displays abrupt

reductions in relative bond capacity, particularly under medium and severe corrosion conditions, indicating a collapse of corrosion-related bond contributions at high temperature.

A direct comparison of the response surfaces highlights a fundamental material-dependent difference in degradation pathways. GPC exhibits a more more monotonic on average bond deterioration trend across the corrosion–temperature domain, whereas PLC shows stronger interaction effects and more abrupt degradation under extreme exposure conditions. These contrasting response characteristics underscore the importance of accounting for material-specific interaction mechanisms when assessing bond performance under combined corrosion and thermal hazards.

4.6 Mechanistic Interpretation of Coupled Effects

The distinct responses observed for GPC and PLC specimens can be attributed to fundamental differences in matrix stability and steel–concrete interfacial behavior under coupled corrosion and thermal exposure. The geopolymer matrix exhibits greater resistance to thermal decomposition than hydrated cement phases, which delays stiffness loss and microstructural degradation at moderate temperatures. As a result, the steel–geopolymer interface appears comparatively less sensitive to localized interfacial deterioration induced by either corrosion or moderate heating. In contrast, the bond performance of PLC relies more strongly on the integrity of the interfacial transition zone (ITZ), which is particularly susceptible to both corrosion-induced cracking and thermally driven microstructural damage. At ambient or moderately elevated temperatures, corrosion products may temporarily enhance bond resistance through increased surface roughness and frictional interaction at the steel–concrete interface. However, under severe thermal exposure, these corrosion products behave as weak and unstable layers, losing cohesion and accelerating interfacial degradation. Simultaneously, thermal incompatibility between steel and the cementitious matrix further compromises confinement and mechanical interlock. The combined influence of these mechanisms leads to a more abrupt reduction in bond capacity and increased variability for PLC specimens under coupled corrosion–temperature exposure. In comparison, the greater thermal stability of the geopolymer matrix and the more gradual evolution of interfacial damage contribute to the smoother and more predictable degradation trends observed for GPC. Together, these mechanistic considerations provide a coherent explanation for the material-dependent differences in bond degradation identified in the preceding sections. Although post-peak behavior was not quantified, qualitative differences provide mechanistic insight complementary to peak load comparisons.

4.7 Conceptual Illustrative Example

This section discusses a simple conceptual example of the proposed methodology. Consider the

assumed simple relation between fire performance and deep uncertain parameters.

$$f_p = x_1 * U_{MP} + x_2 * U_{DC} + x_3 * U_{CC} \quad \text{Eq. 13}$$

where U_{MP}, U_{DC} and U_{CC} are deeply uncertain parameters; f_P is the fire performance; U_{MP} is a deep uncertain parameter due to material properties; U_{DC} is a deep uncertain parameter due to deterioration due to corrosion; U_{CC} is a deep uncertain parameter due to climate change; and x_1, x_2 and x_3 are constants. Here, we can apply Equation 1 to generate the deep uncertain parameters. Here, $\theta_1 = U_{MP}$, $\theta_2 = U_{DC}$, and $\theta_3 = U_{CC}$. Assuming we have some information about the nominal value of $\theta_1, \theta_2, \theta_3$, the following values are considered just for the example problem; θ_1 = 2 its typical range can be 2.0-3.0. The nominal value of θ_2 = 0.73 and its typical range is 0.71- 1.11. The nominal value of θ_3 = 1 and its typical range is 1 – 2. We can generate θ_1, θ_2 and θ_3 values and estimate f_p for different h values, as shown in the table below.

Table 4. Estimation of thetas and fire performance when h = 0.1 and 0.2

f_p		θ_1		θ_2		θ_3	
h=0.1	h=0.2	h=0.1	h=0.2	h=0.1	h=0.2	h=0.1	h=0.2
3.73	3.73	2	2	0.73	0.73	1	1
3.81	3.98	2.01	2.09	0.75	0.79	1.05	1.1
3.9	4.08	2.05	2.1	0.76	0.8	1.09	1.18

To assess the robustness of fire performance under uncertainty, we consider the forecasting of time-dependent uncertain parameters. These parameters can be projected using analytical models or time series techniques to generate plausible intervals over time. In this study, we generate three deeply uncertain parameters θ_1, θ_2, and θ_3 across a range of uncertainty levels defined by a set of horizon values,

$$h = [h_1, h_2, \dots, h_{10}], \ where\ h_1 = 0.1, h_2 = 0.2, \dots\dots\dots\dots, h_{10} = 1.0$$

The uncertain parameters are generated with dimensions [10,1000,50], corresponding to 10

uncertainty horizons, 1000 realizations, and 50 years. A similar three-dimensional matrix is constructed for fire performance, denoted as f_p, with the same shape [10,1000,50]. For each year, we estimate the worst-case fire performance across all realizations for each uncertainty horizon h_i. For example, in year 5, the worst-case fire performances across the horizons are $f_{pw1}, f_{pw2},\ldots, \ f_{pw10}$. If the critical performance threshold is met at the horizon h_5 (i.e., $f_{pw5} = f_{p,critical}$), then the robustness for that year is 50%, indicating that the system can tolerate up to 50% deviation from the nominal values of the uncertain parameters.

Fig. 16a illustrates the relationship between the uncertainty horizon h and fire performance f_p across different years. The trend reveals a decline in robustness over time. For example, robustness is 50% in year 20 and decreases to 20% by year 50. This indicates that by year 50, the design continues to meet performance requirements only if the uncertain parameters do not deviate from their nominal values by more than 20%. In other words, system reliability diminishes as uncertainty increases, underscoring the importance of adaptive or resilient strategies for long-term wildfire risk management.

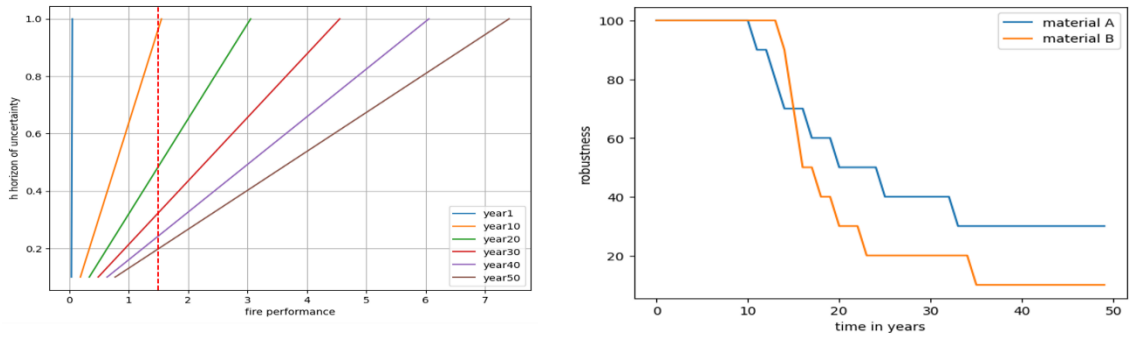

(a) (b)

Fig. 16 (a) h vs f_P for different years showing the critical value; and (b) robustness vs time for two types of concrete

Similarly, to the process described above, we can calculate the fire performance and robustness of two types of concrete PLC and GPC. The difference between the two types of concrete can originate from the material properties, fire resistance, and deterioration models. Fig. 16b shows the robustness of two types of materials. By considering an optimization model with the objective of maximizing the average

robustness over time, we can estimate the robust concrete type. In this simple example, material A is the most robust type. The next step in this project is to plan for dynamic adaptive decision-making. There are three important tasks in this stage to choose a maintenance plan and estimate the decision and forecast horizon. Here, we can consider optimization models to choose the maintenance plans. As described in the previous section, we consider a single objective optimization model by choosing the cost as an objective to choose a maintenance action among those shown in Table 5 below.

Table 5. Fire protection maintenance plans per bridge

Type of Plan	Description	Estimated Cost
Basic Fire Protection Inspection (Strategy A)	Visual inspection of bridge components, including structural elements, electrical systems, and fire detection and suppression systems.	$200 - $500 (per bridge)
Fire detection and suppression systems (Strategy B)	Installing fire detection and suppression systems, such as smoke detectors, sprinklers, and fire extinguishers, to detect and extinguish fires promptly.	$50,000 - $150,000 (per bridge)
Fire Insulation Coating Type-Intumescent coatings (Strategy C)	Expand when exposed to heat, creating a thick, insulating foam layer	$50,000 - $200,000 (per bridge)

By applying the optimization model, we can choose different maintenance strategies over time as shown in Fig. 17, which highlights the selected strategies to be applied over time and tipping points when exceeds the minimum performance level. By continuously adjusting strategies based on real-time information and feedback, systems can achieve and maintain high levels of performance under changing conditions. In fields with rapid technological advancements or evolving trends, dynamic adaptation allows organizations to stay ahead of changes. This ensures that strategies align with the latest developments, fostering innovation and competitiveness. The ability to adapt dynamically supports sustainability initiatives. Organizations can adjust strategies to align with environmental, social, and economic sustainability goals, promoting responsible and resilient practices. As a result, the dynamic adaptation models provide organizations with the tools to navigate uncertainties, respond to changing conditions, and optimize their performance over time. The next step is to choose the forecast horizon, where we can consider robustness as a measure. We can also consider parameter constraints like degradation limits of

the materials, and other uncertain parameters, for example, when we are forecasting traffic demand, traffic demand will have a limit and cannot exceed a critical value for that bridge. We can also consider the accuracy of the forecasting model as a measure of choosing the forecast horizon. For example, if the accuracy of the forecasting model falls below 50% at year 30, then h_{acc} is 30. If the forecasted parameters violate the parameter constraints at year 40, then h_{min} is 40. If the robustness to deep uncertainty is reducing below 50 at year 28, then h_r is 28. Then the forecast horizon would be 28 years. The next step is to predict the decision horizon. For example, the fire performance of the bridge is below the threshold value at year 15. By applying some new policies, the fire performance can be updated, and the updated fire performance falls below the critical value at year 30. At year 25, the cost of the fire performance-enhancing strategy is exceeding the set budget. Let's consider year 20; there is a threshold on the fire-enhancing technology. Then the decision horizon would be 15 years. Decision horizon = (t |min(15, 30, 25, 20, 28)). In this way, we can estimate the decision and forecast horizon. The process is repeated till the end of the life cycle time period.

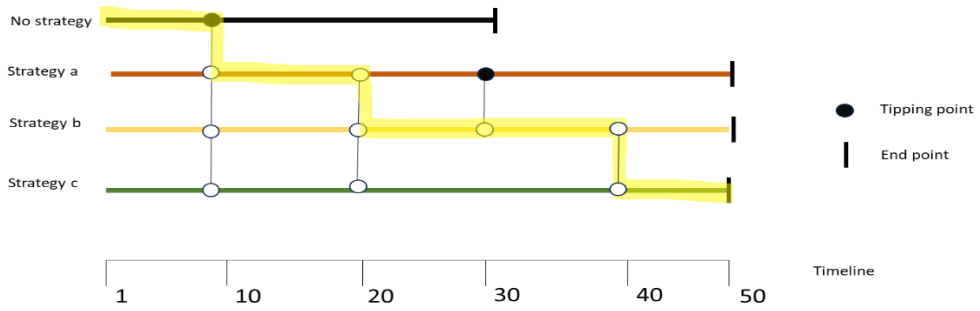

Fig. 17 Dynamic adaptation of strategies over time

Chapter 5. Summary and Conclusions

Based on a systematic experimental investigation of steel–concrete bond behavior under coupled corrosion and thermal exposure and the development of robust, dynamic, and adaptive decision framework, the following conclusions can be drawn:

- Steel–concrete bond performance is strongly influenced by the combined effects of corrosion severity and exposure temperature, and the degradation observed under coupled conditions cannot be reliably inferred from corrosion-only or temperature-only scenarios.
- Peak pull-out load is demonstrated to be a robust and physically meaningful bond performance indicator, applicable to both ductile and brittle bond failure responses and suitable for quantitative comparison across material systems, corrosion levels, and temperature conditions.
- Both PLC and GPC exhibit pronounced bond degradation at severe temperature exposure (800 °C); however, the degradation pathways differ markedly. PLC shows strong interaction effects between corrosion and temperature, including non-monotonic behavior at lower temperatures and abrupt bond deterioration at high temperatures.
- GPC exhibits a more stable, monotonic, and predictable bond degradation trend under combined corrosion and thermal exposure, particularly at elevated temperatures. This behavior is attributed to the higher thermal stability of the geopolymer matrix and reduced sensitivity of the steel–matrix interface to localized interfacial damage.
- Pre-existing corrosion significantly amplifies temperature-induced bond degradation, indicating that temperature-dependent reduction factors commonly used in practice may underestimate bond loss in long-term service conditions where corrosion damage is present.
- The experimentally derived database of peak pull-out loads and relative bond degradation trends provides a validated foundation for probabilistic and reliability-based modeling of bond performance.
- The IGDT component enables a structured exploration of material robustness by accounting for uncertainty envelopes around key parameters such as material degradation and environmental exposure.

- The envelope-bound IG model offers a flexible representation of parameter uncertainty and interdependence, making it well-suited for infrastructure applications with limited or imprecise data.
- The DAPP approach accounts for evolving system needs by identifying tipping points related to fire performance degradation, policy shifts, cost constraints, and technological change.
- A simplified conceptual example demonstrates the application of the methodology, illustrating how robustness varies across uncertainty levels and informing the selection of maintenance actions and adaptation points.

Limitations and Future Work

This study focuses on experimentally characterizing steel–concrete bond degradation in PLC and GPC under discrete corrosion levels and selected exposure temperatures. The corrosion conditions and thermal exposures represent simplified but controlled scenarios and do not capture the full time-dependent evolution of corrosion or the variability of fire exposure in real structures. In addition, peak pull-out load was adopted as the primary bond performance indicator, while other bond-related metrics were not explicitly examined. Future work will extend the present experimental findings by considering time-dependent corrosion progression, alternative thermal histories, and additional bond performance parameters. Microstructural characterization of the steel–concrete interface may also be incorporated to further support the interpretation of the observed degradation trends.

Several limitations of the decision framework should also be acknowledged. The simplified example assumes linear relationships between uncertain variables and performance, which may not capture the full complexity of material behavior under fire and corrosion exposure. The framework also relies on nominal values and parameter ranges that are either hypothetical or literature-based; the accuracy of the robustness and adaptation recommendations will ultimately depend on the quality and representativeness of future experimental inputs. Moreover, the optimization model assumes deterministic cost estimates and does not yet include stochastic cost uncertainty or probabilistic performance degradation models.

Implications for TriDurLE Program Objectives

The results of this study directly support TriDurLE Objective 1 by demonstrating that steel–concrete bond degradation under fire exposure is strongly influenced by pre-existing corrosion and should be treated as a coupled process. The comparative results for PLC and GPC highlight clear material-dependent differences in bond degradation behavior under combined hazards. The experimentally derived bond

performance data provide a quantitative basis for subsequent probabilistic and reliability-based modeling under TriDurLE Objective 2, contributing to the development of life-cycle fire performance assessment frameworks for RC bridges.

References

[1] Ba, G., Miao, J., Zhang, W., & Liu, J. (2019). Influence of reinforcement corrosion on fire performance of reinforced concrete beams. Construction and Building Materials, 213, 738–747. https://doi.org/10.1016/j.conbuildmat.2019.04.065.

[2] Liu, J., Miao, J., Ba, G., Xiao, J., & Hou, D. (2021). Effect of stirrup corrosion and fire on shear behavior of reinforced concrete beams. KSCE Journal of Civil Engineering, 25(9), 3424–3436. https://doi.org/10.1007/s12205-021-1647-8.

[3] S. Chand, V.N. Hsu, S. Sethi, Forecast, solution, and rolling horizons in operations management problems: A classified bibliography, Manufacturing & Service Operations Management, 4 (2002) 25-43.

[4] Kostin, A. M., Guillén-Gosálbez, G., Mele, F. D., Bagajewicz, M. J., & Jiménez, L. (2011). A novel rolling horizon strategy for the strategic planning of supply chains. Application to the sugar cane industry of Argentina. Computers & Chemical Engineering, 35(11), 2540-2563.

[5] Matrosov, E. S., Woods, A. M., & Harou, J. J. (2013). Robust decision making and info-gap decision theory for water resource system planning. Journal of hydrology, 494, 43-58.

[6] Masihabadi, D., Kalantar, M., Majd, Z., & Saravi, S. V. S. (2023). A novel information gap decision theory-based demand response scheduling for a smart residential community considering deep uncertainties. IET Generation, Transmission & Distribution.

[7] Korteling, B., Dessai, S., & Kapelan, Z. (2013). Using information-gap decision theory for water resources planning under severe uncertainty. Water resources management, 27, 1149-1172.

[8] Firouzi, A., Abdolhosseini, M., & Ayazian, R. (2020). Service life prediction of corrosion-affected reinforced concrete columns based on time-dependent reliability analysis. Engineering Failure Analysis, 117, 104944. https://doi.org/10.1016/j.engfailanal.2020.104944

[9] Kirkpatrick, T. J., Weyers, R. E., Anderson-Cook, C. M., & Sprinkel, M. M. (2002). Probabilistic model for the chloride-induced corrosion service life of Bridge Decks. Cement and Concrete Research, 32(12), 1943–1960. https://doi.org/10.1016/s0008-8846(02)00905-5

[10] M.A. Ehlen, A.N. Kojundic, Life-365™ v2. 2, Concrete International, 36 (2014) 41-44.

[11] A. Firouzi, M. Abdolhosseini, R. Ayazian, Service life prediction of corrosion-affected reinforced concrete columns based on time-dependent reliability analysis, Engineering Failure Analysis, 117 (2020).

[12] N.P. Vaddey, D. Trejo, Optimizing test parameters for quantifying critical chloride threshold, ACI

Materials Journal, 118 (2021) 53-65.

[13] G. Ba, J. Miao, W. Zhang, J. Liu, Influence of reinforcement corrosion on fire performance of reinforced concrete beams, Construction and Building Materials, 213 (2019) 738-747.

[14] S. Timilsina, N. Yazdani, E. Beneberu, Post-fire analysis and numerical modeling of a fire-damaged concrete bridge, Engineering Structures, 244 (2021).

[15] W. Wright, B. Lattimer, M. Woodworth, M. Nahid, E. Sotelino, National Cooperative Highway Research Program (NCHRP), Transportation Research Board, National Research Council, and The National Academies, in: H.B.F.H.A.D.F. Report (Ed.), National Cooperative Highway Research Program (NCHRP), Blacksburg, VA, 2013.

[16] T.J. Kirkpatrick, R.E. Weyers, C.M. Anderson-Cook, M.M. Sprinkel, Probabilistic model for the chloride-induced corrosion service life of bridge decks, Cement and Concrete Research, 32 (2002) 1943-1960.

[17] R. Vergoossen, A. Wolfert, E. Koenders, Objective risk based structural assessment of existing concrete structures, Life-Cycle of Engineering Systems: Emphasis on Sustainable Civil Infrastructure, CRC Press2016, pp. 1406-1413.

[18] J. Taheri-Shakib, A. Al-Mayah, Dynamics of localized accelerated corrosion in reinforced concrete: Voids, corrosion products, and crack formation, Ceramics International, 50 (2024) 48755-48767.

[19] N. Anita, R.M. Joany, R. Dorothy, J. Aslam, S. Rajendran, A. Subramania, G. Singh, C. Verma, Chapter 4 - Linear polarization resistance (LPR) technique for corrosion measurements, in: J. Aslam, C. Verma, C. Mustansar Hussain (Eds.) Electrochemical and Analytical Techniques for Sustainable Corrosion Monitoring, Elsevier2023, pp. 59-80.

[20] E. McCafferty, Validation of corrosion rates measured by the Tafel extrapolation method, Corrosion Science, 47 (2005) 3202-3215.

[21] U. Angst, M. Büchler, On the applicability of the Stern–Geary relationship to determine instantaneous corrosion rates in macro-cell corrosion, Materials and Corrosion, 66 (2014) 1017-1028.

[22] Y. Liu, X. Hu, Y. Du, B. Nematollahi, C. Shi, A review on high-temperature resistance of geopolymer concrete, Journal of Building Engineering, 98 (2024).

[23] M. Amran, S.-S. Huang, A.M. Onaizi, G. Murali, H.S. Abdelgader, Fire spalling behavior of high-strength concrete: A critical review, Construction and Building Materials, 341 (2022).

[24] A. Ergün, G. Kürklü, M.S. Başpınar, The effects of material properties on bond strength between reinforcing bar and concrete exposed to high temperature, Construction and Building Materials, 112

(2016) 691-698.

[25] F. Tariq, P. Bhargava, Bond characteristics of corroded pullout specimens exposed to elevated temperatures, Structures, 25 (2020) 311-322.

[26] J. Liu, J. Miao, G. Ba, J. Xiao, D. Hou, Effect of Stirrup Corrosion and Fire on Shear Behavior of Reinforced Concrete Beams, KSCE Journal of Civil Engineering, 25 (2021) 3424-3436.

[27] S.S. Roudsari, T.M. Abu-Lebdeh, Evaluation of Fire Effects on Reinforced Concrete Columns Using Finite Element Method, American Journal of Engineering and Applied Sciences, 12 (2019) 227-235.

[28] R. Salehi, A. Akbarpour, A. Shalbaftabar, Fire Evaluation of RC Frames Strengthened with FRPs Using Finite Element Method, American Journal of Engineering and Applied Sciences, 13 (2020) 610-626.

[29] J. Feng, K. Gao, W. Gao, Y. Liao, G. Wu, Machine learning-based bridge cable damage detection under stochastic effects of corrosion and fire, Engineering Structures, 264 (2022).

[30] Z. Lounis, T.P. McAllister, Risk-Based Decision Making for Sustainable and Resilient Infrastructure Systems, Journal of Structural Engineering, 142 (2016).

[31] S. Luhar, D. Nicolaides, I. Luhar, Fire Resistance Behaviour of Geopolymer Concrete: An Overview, Buildings, 11 (2021).

[32] M. Amran, S.-S. Huang, S. Debbarma, R.S.M. Rashid, Fire resistance of geopolymer concrete: A critical review, Construction and Building Materials, 324 (2022).

[33] P.K. Sarker, S. Kelly, Z. Yao, Effect of fire exposure on cracking, spalling and residual strength of fly ash geopolymer concrete, Materials & Design, 63 (2014) 584-592.

[34] T. Manzoor, J.A. Bhat, A.H. Shah, Performance of geopolymer concrete at elevated temperature − A critical review, Construction and Building Materials, 420 (2024).

[35] H. Yu, K.-T.K. Chiang, L. Yang, Threshold chloride level and characteristics of reinforcement corrosion initiation in simulated concrete pore solutions, Construction and Building Materials, 26 (2012) 723-729.

[36] Marchau, V.A.W.J., Walker, W.E., Bloemen, P.J.T.M., & Popper, S.W. (2019). Decision making under deep uncertainty: from theory to practice. Springer, Switzerland. https://doi.org/10.1007/978-3-030-05252-2_18.

[37] Amran, M., Huang, S. S., Debbarma, S., & Rashid, R. S. (2022). Fire resistance of geopolymer concrete: A critical review. Construction and Building Materials, 324, 126722.

[38] Luhar, S., Nicolaides, D., & Luhar, I. (2021). Fire resistance behaviour of geopolymer concrete: An

overview. Buildings, 11(3), 82.

[39] Sarker, P.K.; Kelly, S.; Yao, Z.T. (2014). Effect of fire exposure on cracking, spalling and residual strength of fly ash geopolymer concrete. Mater. Des. 63, 584–592

[40] Q. Ma, R. Guo, Z. Zhao, Z. Lin, K. He, Mechanical properties of concrete at high temperature—A review, Construction and Building Materials, 93 (2015) 371-383.